NREL
NATIONAL RENEWABLE ENERGY LABORATORY

Using Whole-House Field Tests to Empirically Derive Moisture Buffering Model Inputs

J. Woods, J. Winkler, and D. Christensen
National Renewable Energy Laboratory

E. Hancock
Mountain Energy Partnership

NREL is a national laboratory of the U.S. Department of Energy
Office of Energy Efficiency & Renewable Energy
Operated by the Alliance for Sustainable Energy, LLC

This report is available at no cost from the National Renewable Energy Laboratory (NREL) at www.nrel.gov/publications.

Technical Report
NREL/TP-5500-62456
August 2014

Contract No. DE-AC36-08GO28308

NREL
NATIONAL RENEWABLE ENERGY LABORATORY

Using Whole-House Field Tests to Empirically Derive Moisture Buffering Model Inputs

J. Woods, J. Winkler, and D. Christensen
National Renewable Energy Laboratory

E. Hancock
Mountain Energy Partnership

Prepared under Task No. BE12.2046

National Renewable Energy Laboratory
15013 Denver West Parkway
Golden, CO 80401
303-275-3000 • www.nrel.gov

Technical Report
NREL/TP-5500-62456
August 2014

Contract No. DE-AC36-08GO28308

NOTICE

This report is available at no cost from the National Renewable Energy Laboratory (NREL) at www.nrel.gov/publications.

Available electronically at http://www.osti.gov/scitech

Available for a processing fee to U.S. Department of Energy and its contractors, in paper, from:

U.S. Department of Energy
Office of Scientific and Technical Information
P.O. Box 62
Oak Ridge, TN 37831-0062
phone: 865.576.8401
fax: 865.576.5728
email: mailto:reports@adonis.osti.gov

Available for sale to the public, in paper, from:

U.S. Department of Commerce
National Technical Information Service
5285 Port Royal Road
Springfield, VA 22161
phone: 800.553.6847
fax: 703.605.6900
email: orders@ntis.fedworld.gov
online ordering: http://www.ntis.gov/help/ordermethods.aspx

Cover Photos: (left to right) photo by Pat Corkery, NREL 16416, photo from SunEdison, NREL 17423, photo by Pat Corkery, NREL 16560, photo by Dennis Schroeder, NREL 17613, photo by Dean Armstrong, NREL 17436, photo by Pat Corkery, NREL 17721.

Acknowledgments

This work was supported by the U.S. Department of Energy under Contract No. DE-AC36-08-GO28308 with the National Renewable Energy Laboratory. The authors would like to thank Greg Barker (Mountain Energy Partnership) for his help with data acquisition, Jeff Tomerlin (the National Renewable Energy Laboratory) for his help in building the laboratory-scale chamber, as well as David Hoak and Eric Martin (Florida Solar Energy Center) for their help with the test setup at the Florida test home.

Nomenclature

A	surface area (m^2)
C	molar concentration (kmol $kmol^{-1}$)
d_{EMPD}	effective moisture penetration depth (m)
h_m	mass transfer coefficient (kg m^{-2} s^{-1})
k	mass transfer coefficient (m s^{-1})
M	molar mass (kg $kmol^{-1}$)
M_v	cumulative transfer of vapor/moisture (kg)
$\dot{m}$	mass flow rate (kg s^{-1})
$\dot{m}_v$	mass flow rate of vapor/moisture (kg s^{-1})
m_r	rate of increase of humidity at beginning of tests (%RH s^{-1})
N	number of moles (kmol)
n	molar flow rate (kmol s^{-1})
P	pressure (Pa)
p_{sat}	saturation vapor pressure (Pa)
T	temperature (°C)
t	time (s)
V	volume (m^3)
w	material moisture content (kg m^{-3})
δ	vapor permeability (kg m^{-1} Pa^{-1} s^{-1})
μ	vapor resistance factor; ratio of vapor permeability in a material to that in air
Π	lumped parameter for empirical model
ϕ	relative humidity
ω	humidity ratio (kg kg^{-1})

Subscripts

amb condition/property of the ambient air

deep deep layer of the EMPD model

gain moisture added from internal gains or with humidifier

gen generated/injected

HVAC moisture removed with either air conditioner or dehumidifier

inf infiltration

matl material

scale mass measured by scale

surf surface layer of the EMPD model

zone condition/property of the house zone air

Abbreviations

CO_2 carbon dioxide

EC effective capacitance

EMPD effective moisture penetration depth

FSEC Florida Solar Energy Center

HVAC heating, ventilation, and air conditioning

RH relative humidity

Executive Summary

Building energy simulations can be used to predict a building's interior conditions, along with the energy use associated with keeping these conditions comfortable. These models simulate the loads on the building (e.g., internal gains, envelope heat transfer), determine the operation of the space conditioning equipment, and then calculate the building's temperature and relative humidity (RH) throughout the year. The indoor temperature and RH are affected not only by the loads and the space conditioning equipment, but also by the capacitance of the building materials, which buffer changes in temperature and humidity.

The thermal capacitance is typically included in these models, because it can strongly affect energy use. The moisture capacitance has a smaller effect on energy use, and the modeling of moisture capacitance is either simple (and inaccurate) or nonexistent in most building energy simulation programs. But this moisture capacitance has become increasingly important for modeling residential buildings because higher efficiency building codes have led to reduced sensible loads without a corresponding decrease in the moisture (latent) load. Researchers and builders are actively studying humidity control in homes, either through energy recovery ventilators, stand-alone dehumidifiers, or packaged air-conditioning systems with enhanced dehumidification.

This research developed an empirical method to extract whole-house model inputs for use with a more accurate moisture capacitance model (the effective moisture penetration depth, or EMPD, model). The experimental approach was to subject the materials in the house to a square-wave RH profile, measure all the moisture transfer terms (e.g., infiltration, air conditioner condensate), and calculate the only unmeasured term: the moisture sorption into the materials. After validating the method with laboratory measurements, we performed the tests in a slab-on-grade house with concrete block walls at the Florida Solar Energy Center in Cocoa, Florida. We used a least-squares fit of an analytical solution to the measured moisture sorption curves to determine the three independent model parameters representing the moisture buffering potential of this house and its furnishings.

After deriving these parameters, we measured the RH of the same house during tests with realistic latent and sensible loads, and then compared that to the RH predicted by the EMPD model using these inputs. This showed good agreement (Figure ES-1(a)), especially compared to the commonly used effective capacitance approach (Figure ES-1(b)). Even if we adjust the single parameter used in the effective capacitance model to try and match the data, we can only improve the R2 from 0.40 (for a commonly used effective capacitance of 10) to 0.52 (effective capacitance ~5). Both are considerably worse than the EMPD model (R2 = 0.81).

These results show that the EMPD model, once the inputs are known, is an accurate moisture buffering model. A sensitivity analysis showed that the model is fairly insensitive to changes in the model inputs up to 20%.

This experimental method can be used in houses of other constructions (e.g., wood frame), and with other levels of furnishings, to develop a more comprehensive dataset. This can provide guidance on moisture buffering model inputs for use in building simulations, such that the indoor RH can be predicted with greater accuracy. This can help answer questions about the effects of insulation levels, cooling equipment selection, and ventilation practices on the indoor RH, and help anticipate potential problems.

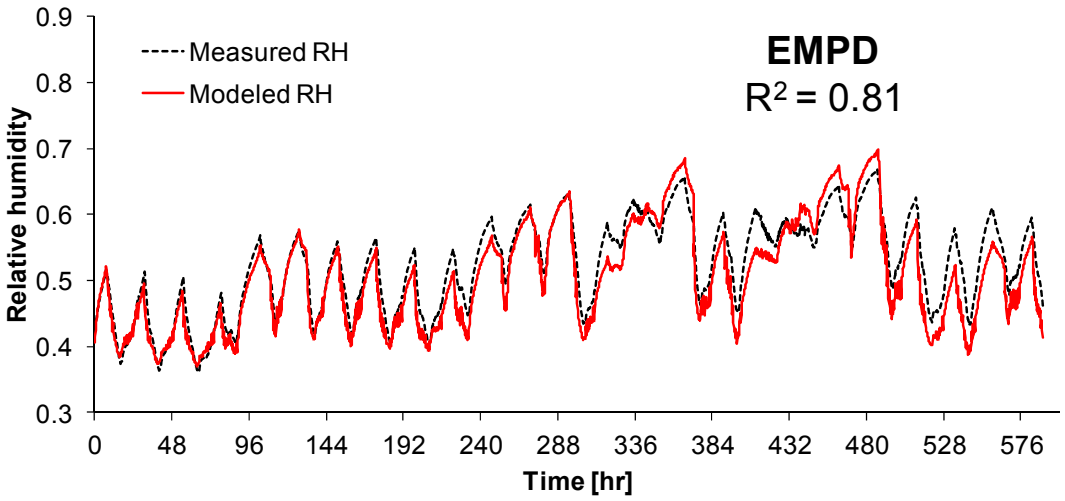

(a)

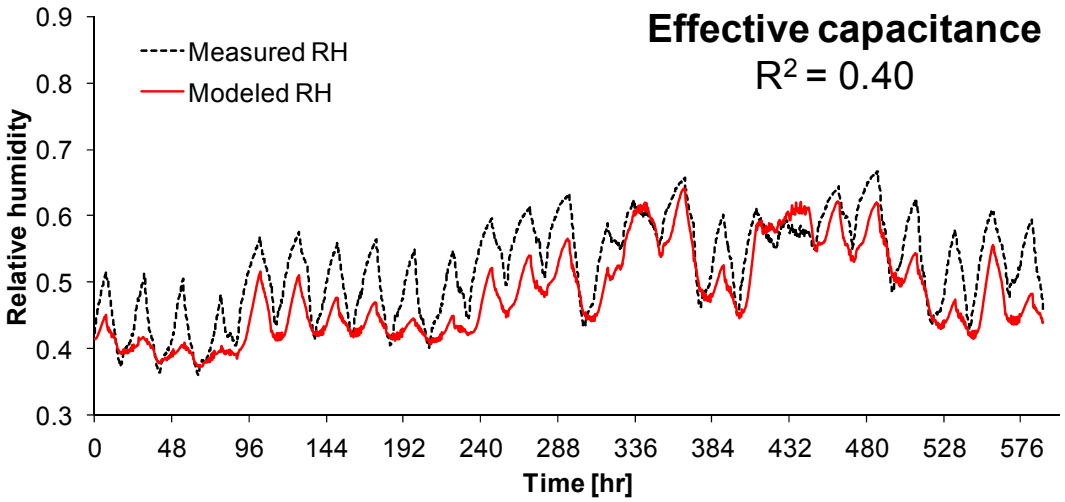

(b)

Figure ES-1: Comparison of measured relative humidity to modeled relative humidity. (a) EMPD model with inputs derived using new method used in this paper, (b) effective capacitance model with commonly-used value effective capacitance value of 10.

Table of Contents

List of Figures

Unless indicated otherwise, all photos and graphics were created by the authors.

List of Tables

1 Introduction

Building energy simulation models use the principles of heat and mass transfer to provide essential information to building researchers, designers, and engineers. These models can predict the temperature and humidity inside a building and the energy use associated with keeping these conditions comfortable, given an appropriate set of parameters and inputs. They can also be used to study the effects of design options on energy use and interior conditions.

To calculate a building's interior conditions, the building energy models must estimate the latent and sensible loads on the building (e.g., infiltration, internal gains, envelope heat transfer) and the performance of any space conditioning equipment. The model also needs to consider the capacitance of the materials in the building, which buffer the response of the interior conditions to these loads. For example, a sensible load will change the air temperature in an empty house with lightweight walls more quickly than in a furnished house with heavy walls, such as masonry, because much of the thermal energy is stored in the furnishings and the heavy walls, rather than in the air. This can have a considerable effect on energy use, as the diurnal variation in temperature can be buffered by this thermal capacitance, and is included in many building energy models.

Similar to the thermal capacitance's effect on temperature, the moisture capacitance of a building's materials is important for predicting the interior relative humidity (RH). The materials absorb[1] or release moisture depending on the RH of the surrounding air. This buffers changes to the air humidity. These calculations of moisture storage and transport are often simplified or ignored in building energy models. Although the simplified models adequately predict energy use in many cases [1], they do not adequately predict the interior RH. Predicting RH has become important as improvements to the building envelope and lighting have reduced the sensible load, while the latent load from internal gains and required ventilation has remained relatively constant [2, 3]. This can result in increased RH, and may require dehumidification equipment. Accurately predicting the interior RH is essential to understanding these potential problems and to properly evaluating and selecting potential solutions.

The simplest method for including moisture capacitance in modeling is to increase the capacitance of the air in the building to account for the added capacitance of the materials. This effective capacitance (EC) model assumes that the volume of the air in the building is 10–15 times larger than the actual volume. This model is unrealistic and cannot be calibrated to give an accurate RH response [1].

A complex method for studying moisture capacitance and moisture flows in building modeling is the finite difference method, which spatially discretizes the differential equations within the material [4, 5]. This approach is accurate, but requires long simulation times.

Another approach is the effective moisture penetration depth (EMPD) model [6-8]. The EMPD model assumes that the moisture transfer takes place between the zone air and a thin fictitious

[1] Moisture *ad*sorption onto a material's surface (including its internal pore structure) and *ab*sorption into the bulk material are collectively known as *sorption*. Both adsorption and absorption occur in building materials (adsorption at lower humidity, absorption at higher humidity). In this report, we use the following terms to collectively refer to either adsorption or absorption: *sorption*, *absorption*, and *absorb*.

layer of uniform moisture content. The basis for this model is that the zone RH is cyclical. If it is perfectly cyclical (e.g., a sine wave), the model gives nearly the exact solution. If it is not perfectly cyclical, it can still be a good approximation [9]. The EMPD model offers a more realistic approach than the EC model and a simpler approach than the finite-difference method.

The EMPD model still requires more complicated inputs than the EC model, which simply uses a multiplier on the zone air capacitance. The EMPD model requires the moisture properties (permeability, moisture sorption curve, etc.) and the surface areas for each material in the house. It is possible, though, to measure a material's bulk EMPD properties, as demonstrated by several researchers [10-12]. In 2011, Vereecken et al. [13] demonstrated an experimental method for measuring a single set of EMPD model inputs for multiple materials at once.

In this research, we modified that experimental method so it could be extended to measuring the moisture buffering model inputs for a whole house. We first verified the accuracy of the method with laboratory-scale experiments on materials with known moisture properties. We then measured the moisture buffering of a whole house, and derived the necessary model inputs for building energy simulations. We validated the model with additional experiments on the same house with simulated occupants.

In this report, we describe the experimental setup and present results for these experiments. Before this, we give a brief primer on moisture modeling with the EMPD model.

2 The EMPD Model

The primary equation for modeling moisture in buildings comes from a moisture balance on the zone air:

$$\rho_{air} V_{zone} \frac{d\omega_{zone}}{dt} = \dot{m}_v\big|_{\text{inf}} + \dot{m}_v\big|_{\text{gain}} - \dot{m}_v\big|_{\text{HVAC}} - \dot{m}_v\big|_{\text{matl}} \quad (1)$$

where ρ_{air} is the air density, V_{zone} the zone volume, and ω_{zone} the zone humidity ratio. Each term on the right-hand side is a moisture exchange [kg/s] with the zone air:

$\dot{m}_v\big|_{\text{inf}}$ moisture entering the zone due to infiltration

$\dot{m}_v\big|_{\text{gain}}$ moisture entering the zone due to internal moisture generation

$\dot{m}_v\big|_{\text{HVAC}}$ moisture exiting the zone as condensate at an air conditioner or dehumidifier

$\dot{m}_v\big|_{\text{matl}}$ moisture exiting the zone due to moisture sorption by the materials in the zone

The focus of this research is on the last term: moisture exchange with the building's materials. The EMPD model is one way to calculate this term, if the moisture properties of the materials are known. The EMPD model can be visualized with Figure 1. The material-air coupling takes place through a resistance between the zone air and a *surface layer*, which is a fictitious layer with an

assumed uniform moisture content. This surface layer is also connected to a *deep layer* through a second resistance. The surface layer responds relatively quickly to changes in RH, and therefore dampens higher frequency changes in the zone RH (e.g., daily fluctuations from daytime air conditioner use). The deep layer typically has a higher capacitance for moisture storage, but responds more slowly. It dampens lower frequency changes in the zone RH (e.g., changes in the weather).

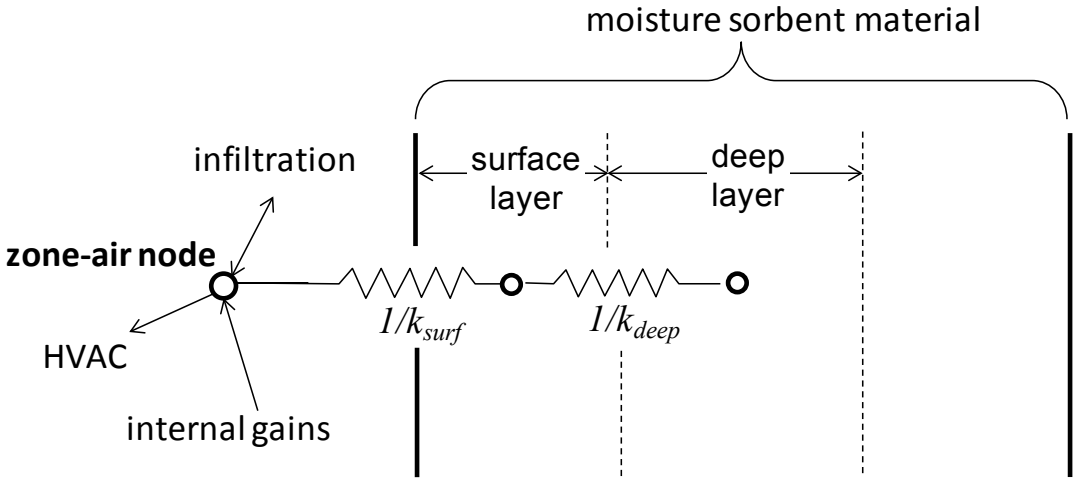

Figure 1. EMPD model schematic

The moisture exchange between the zone air and the surface layer is calculated with:

$$\dot{m}_v\big|_{\text{matl}} = h_m A\left(\omega_{zone}(t) - \omega_{surf}(t)\right) \tag{2}$$

where h_m is the mass transfer coefficient, A the surface area of the material, and ω_{surf} the humidity ratio of the surface layer. Note that this humidity ratio is not a realistic quantity. Instead, this value can be thought of as the humidity ratio of air in equilibrium with the moisture content of the surface layer (w_{surf} [kg/m^3]). These are related through the material's moisture sorption curve. If we assume the curve is linear with RH, which is a reasonable assumption for the RH range typically seen in buildings (20%–80%), these two quantities are related with:

$$w_{surf} = \frac{dw}{d\phi}\frac{P\omega_{surf}}{p_{sat}\left(0.622+\omega_{surf}\right)} \tag{3}$$

where $dw/d\phi$ is the slope of the moisture sorption curve, P the absolute pressure, and p_{sat} the saturated vapor pressure. In the EMPD model, the moisture content of the surface and deep layers needs to be calculated at each time step. This is done with a moisture balance on each layer:

$$Ad_{EMPD}\frac{dw_{surf}(t)}{dt} = k_{surf}A\left(w_{zone}(t) - w_{surf}(t)\right) \tag{4}$$

$$Ad_{EMPD-deep}\frac{dw_{deep}(t)}{dt} = k_{deep}A\left(w_{surf}(t) - w_{deep}(t)\right) \tag{5}$$

where k_{surf}, w_{surf}, and d_{EMPD} are the mass transfer coefficient, moisture content, and effective moisture penetration depth for the surface layer, and k_{deep}, w_{deep}, and $d_{EMPD\text{-}deep}$ the corresponding values for the deep layer. Note that these mass transfer coefficients, which are based on a material moisture content driving force, differ from that used in Eq. (2), which is based on a humidity ratio driving force. In this case, we've used Eq. (3) to link the zone humidity ratio (ω_{zone}) with the material moisture content in equilibrium with the zone humidity ratio (w_{zone}). The mass transfer coefficients are defined as [9]:

$$k_{surf} = \frac{2\delta_{matl} p_{sat}}{dw/d\phi \, d_{EMPD}} = \frac{2\delta_{air} p_{sat}}{dw/d\phi \, d_{EMPD} \mu} \tag{6}$$

$$k_{deep} = \frac{1}{\frac{1}{k_{surf}} + \frac{dw/d\phi \, d_{EMPD-deep}}{2\delta_{matl} p_{sat}}} = \frac{1}{\frac{1}{k_{surf}} + \frac{dw/d\phi \, d_{EMPD-deep} \mu}{2\delta_{air} p_{sat}}} \tag{7}$$

where δ_{matl} and δ_{air} are the vapor permeability of the material and the air, respectively, and μ is the ratio between these permeabilities, termed the *vapor resistance factor*:

$$\mu = \frac{\delta_{air}}{\delta_{matl}} \tag{8}$$

These equations represent the EMPD model. By discretizing the time derivatives, the equations can be solved to determine the moisture exchange between the zone air and the materials. The moisture properties in these equations must also be known. This is the focus of the remainder of this report: determining the moisture property inputs for the EMPD model based on whole-house field tests.

3 Methods

The methods for this research can be split into three areas: (1) the experiments used to measure the moisture exchange between the air and materials of a house due to a prescribed RH profile; (2) the analysis that takes these data and empirically derives the input parameters for the EMPD moisture buffering model; and (3) tests on the house with realistic sensible and latent load profiles, which is used to validate the empirically derived parameters and the EMPD model.

3.1 Experimental Approach

For our experimental approach, we calculate the moisture sorption into (and desorption from) the building's materials by rearranging Eq. (1):

$$\dot{m}_v\big|_{\text{matl}} = -\rho_{air} V_{zone} \frac{d\omega_{zone}}{dt} + \dot{m}_v\big|_{\text{inf}} + \dot{m}_v\big|_{\text{gain}} - \dot{m}_v\big|_{\text{HVAC}} \tag{9}$$

where $\dot{m}_{v,matl}$ is the moisture transfer rate into the materials. We can integrate this equation from time $t = 0$ to time t to get the cumulative moisture transfer into the materials:

$$M_{v,matl} = -M_{v,air} + M_{v,inf} + M_{v,gain} - M_{v,HVAC} \tag{10}$$

Where

$$M_{v,matl} = \int_0^t \dot{m}_v\big|_{\text{matl}}(t)dt \tag{11}$$

$$M_{v,air} = \rho_{air} V_{zone}\left(\omega_{zone}(t) - \omega_{zone}(0)\right) \tag{12}$$

$$M_{v,inf} = \int_0^t \dot{m}_{air,inf}(t)\left(\omega_{amb}(t) - \omega_{zone}(t)\right)dt \tag{13}$$

$$M_{v,gain} = \int_0^t \dot{m}_v\big|_{\text{gain}}(t)dt \tag{14}$$

$$M_{v,HVAC} = \int_0^t \dot{m}_v\big|_{\text{HVAC}}(t)dt \tag{15}$$

If we measure all the right-hand-side terms in Eq. (10), we can calculate how much moisture is being absorbed into the materials. Figure 2 illustrates the experimental setup, and indicates the positive direction of each term in Eqs. (9) and (10). The details of these measurements are discussed in Section 3.1.1.

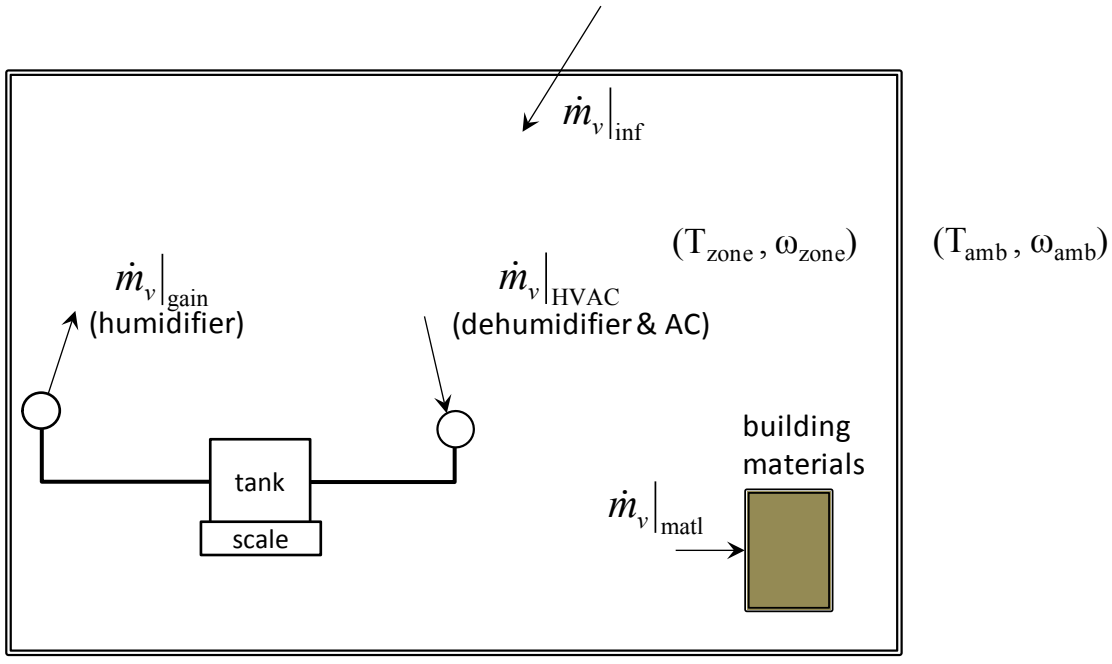

Figure 2. Experimental approach, showing each term in Eq. (9). Arrows indicate the positive direction for each term. Measurement techniques are explained in Section 3.1.1.

The tests used a square-wave RH profile (Figure 3a), which gives a strong forcing function. This is not a perfect square wave because of the finite addition and removal of moisture by the humidifier and dehumidifier, with the transient period on the order of 1 hour. An example curve

for the cumulative moisture sorption (Mv,matl) is shown in Figure 3b, with the materials absorbing moisture during high RH periods ($\dot{m}v|matl > 0$), and desorbing moisture during low RH periods ($\dot{m}v|matl < 0$).

These tests were performed in both a tightly controlled laboratory setting (Section 3.1.2), and in a well-characterized test house (Section 3.1.3). The former was used to validate the experimental setup, and the latter was used to obtain data to derive the EMPD model inputs for a whole house.

The square wave in Figure 3 has a cycle period of 24 hours, which was used to measure the response of the materials to high-frequency changes in RH. We also tested with a cycle period of 2 weeks (tests were performed serially, not concurrently) to determine the response to low-frequency changes. In the EMPD model, these two responses are handled with the surface layer and the deep layer, as discussed in Section 2.

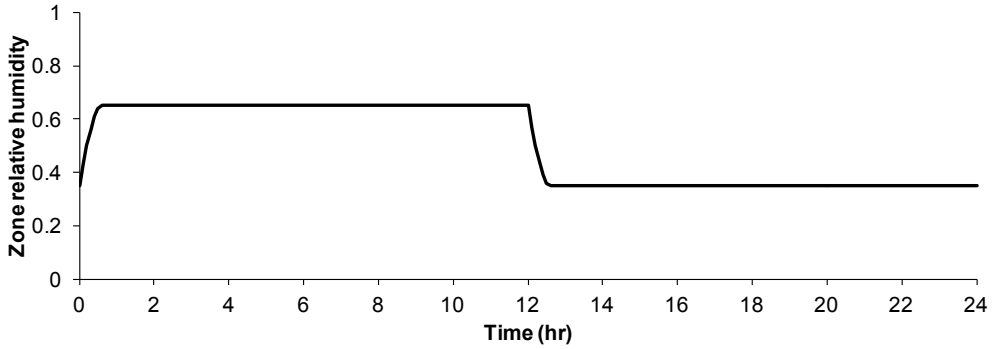

(a)

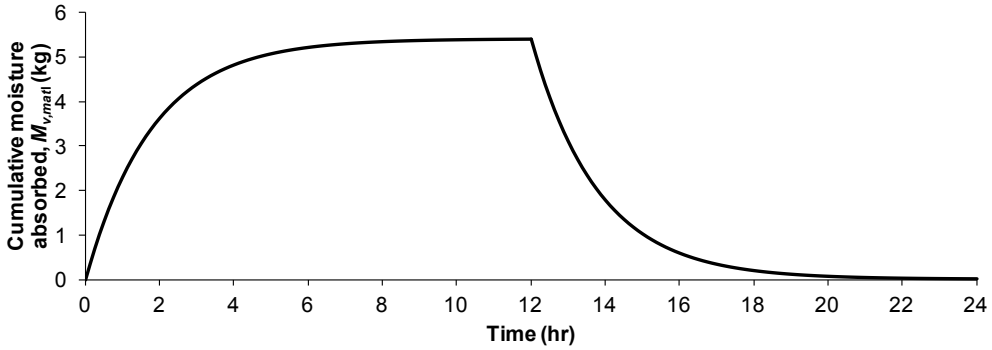

(b)

Figure 3. Test profiles for (a) RH (input) and (b) illustrative cumulative moisture sorption (output)

This test method differs from the method of Vereecken et al. [13] in a few key ways:

They measured the moisture added with the humidifier (Mv,gain) and the moisture in the zone air (Mv,air). They did not remove moisture from the space (Mv,HVAC) and did not measure infiltration moisture (Mv,inf). Instead, the RH of the space decayed because of infiltration during times when the humidifier was off, and they inferred the infiltration rate based on this decay rate. This assumes the infiltration rate and ambient humidity are relatively constant. In the method used here, we removed moisture with a dehumidifier during the low RH periods, and used an air conditioner for cooling, to maintain a constant temperature. We also measured the infiltration

rate directly. This enabled the use of this method in the field, even for a house in a hot-humid climate. It also gave a cleaner signal, because the infiltration moisture transfer, which can vary with time, was measured continuously via tracer gas rather than derived from the data.

Because we actively dehumidified during the low RH periods, we obtained a RH profile close to square waves. This allows a simpler data reduction method, with its clean step function changes compared to the slowly decaying RH profile used in Vereecken et al. [13].

The final key difference is that we measured the response to both short (24-hour) and long (2-week) cycles, and derived a surface layer thickness (from the 24-hour tests) and a deep layer thickness (from the 2-week long tests). As we show in Section 4.4, this deep layer significantly improves the accuracy of the model.

3.1.1 Experimental Setup

The house used for the experiments is in Cocoa, Florida, at the Florida Solar Energy Center (Figure 4). It is one of two houses that comprise the Flexible Residential Test Facility [14], built in 2010. These houses are single story, slab-on-grade construction with painted, uninsulated concrete block walls, and R-19 attic insulation. The inside of the exterior walls has furring strips and painted drywall. The 1536-ft2 floor area is one large room, with (initially) no interior walls or furnishings. Air infiltration can be adjusted using configurable leakage points and was less than 2.5 ACH50 for this study.

Figure 4. Test house at Florida Solar Energy Center for whole-house tests

For the moisture buffering tests, we made some modifications to ensure accurate moisture measurements. The windows were covered and sealed with rigid foam insulation to prevent condensation on the single-pane windows during the cool winter months, and to minimize any impacts from solar heating. The house air conditioner (located in the garage) was turned off, with the supply and return registers sealed. A separate air conditioner, along with the minimal

ductwork for distribution, was installed inside the conditioned space. This eliminated any possible leakage between the attic ducts and the unconditioned attic, which would have resulted in unmeasured moisture transfer.

As described in the previous section, the RH forcing function consisted of square waves of two different frequencies. A humidifier and dehumidifier increased and decreased the RH to meet these square wave profiles, while electric heaters and an air conditioner maintained a constant zone temperature. The key measurements (terms in Eq. (10)) and the measuring instruments used in the whole-house tests are listed in Table 1; the equipment used to control temperature and RH is listed in Table 2. A brief description of the key measurements used in the whole-house test follows.

Table 1. List of Measurement Method/Instrumentation for Whole-House Field Tests

Measurement	Measurement method/instrumentation
Zone humidity ($M_{v,air}$)	Vaisala HMP-110 Temperature and RH sensor (±0.2 °C; ±1.7% RH)
Infiltration ($M_{v,inf}$)	Continuous CO_2 tracer gas (Dakota mass flow meter (±0.075 L/min) and GE Ventostat CO_2 concentration transmitters (±3%)
Moisture addition ($M_{v,gain}$)	Sartorius Signum 35-kg scale (±0.001 kg)
Moisture removal ($M_{v,HVAC}$)	Sartorius Signum 35-kg scale (±0.001 kg)
Material sorption ($M_{v,matl}$)	None (calculated from above measurements)

Table 2: List of Equipment for Whole-House Field Tests

Humidifier	Humidifirst MP-15
Dehumidifier	Ultra-Aire XT155H
Air conditioner	Nordyne 3-ton heat pump (condenser: FT4BD; air handler: GB5BM)
Heater(s)	(4) 1500-W electric ceramic heaters

Zone air ($M_{v,air}$): To measure the humidity of the zone air, we divided the zone into four quadrants and placed temperature and RH sensors in the center of each quadrant, 4 ft above the floor. The zone air was assumed to be well-mixed, with four ceiling fans and two small floor fans continuously operating. The zone air was calculated as the average of the four temperature and RH sensor measurements; however, the spatial distribution of humidity throughout the house was small.

Infiltration ($M_{v,inf}$): Moisture infiltration was calculated as the difference between the indoor and outdoor humidity ratio, multiplied by the infiltration mass flow rate. The mass flow rate was measured with a continuous CO_2 tracer gas, which was already in use by Florida Solar Energy Center researchers for previous, unrelated experiments. CO_2 was continuously metered into the space at approximately 0.4 L/min. This flow rate was measured with a mass-flow meter, while the zone and ambient CO_2 concentration was measured with two CO_2 concentration sensors. Because sensor drift is often a problem with CO_2 sensors, they were checked and recalibrated every few months during the experiment.

The concentration measurements and the known release rate were used to calculate the infiltration flow rate from a CO_2 balance on the house:

$$N_{zone}\frac{dC_{zone}}{dt} = n_{gen} - n_{inf}\left(C_{zone} - C_{amb}\right) \tag{16}$$

where N_{zone} is the total number of moles of air in the zone, n_{gen} is the injection rate of CO_2 into the zone, n_{inf} is the air infiltration rate ($kmol_{air}/s$), and C_{zone} and C_{amb} are the CO_2 concentrations ($kmol_{CO2}/kmol_{air}$) for the zone and ambient air, respectively.

Solving this equation for the infiltration rate gives:

$$n_{inf} = \frac{n_{gen} - N_{zone}\dfrac{dC_{zone}}{dt}}{C_{zone} - C_{amb}} \tag{17}$$

This infiltration was converted to a mass flow by multiplying by the molar mass of air (M_{air} = 28.97 kg/kmol):

$$\dot{m}_{air,inf} = \mathrm{M}_{\mathrm{air}} n_{inf} \tag{18}$$

Gains and removals ($M_{v,gain}$ and $M_{v,HVAC}$): Moisture was added to or removed from the space to match the prescribed RH profile (Figure 3a). We measured these additions and removals by weighing a tank of water, which supplied the humidifier with water and collected condensate from the air conditioner and dehumidifier (Figure 5). The humidifier was placed on the scale because of its non-negligible storage capacity. This leads to a simple equation for the moisture gains and removals:

$$M_{v,gain}(t) - M_{v,HVAC}(t) = M_{scale}(0) - M_{scale}(t) \tag{19}$$

where time $t = 0$ is the time at the start of a RH cycle.

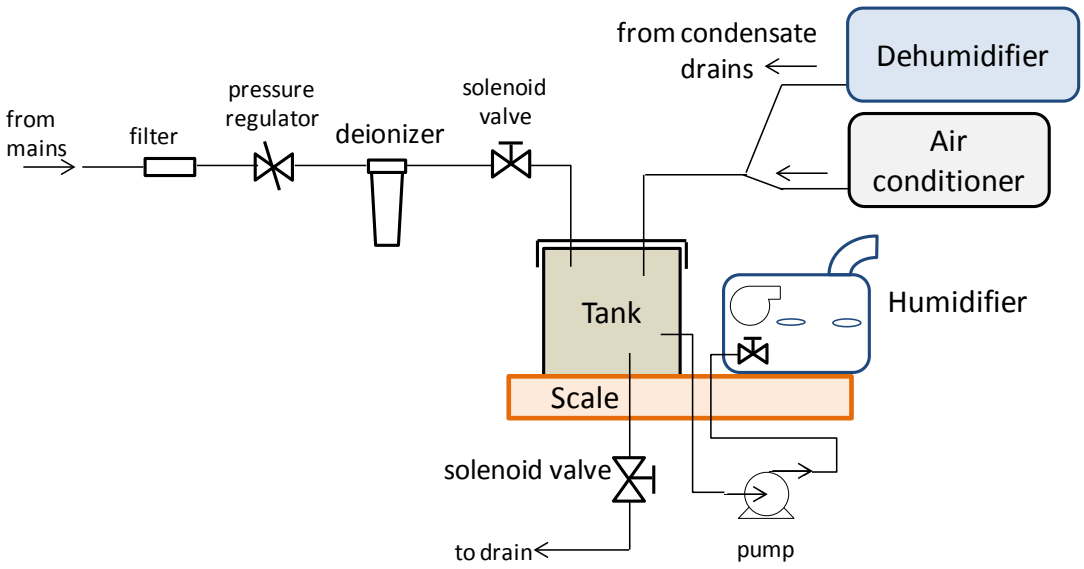

Figure 5. Equipment setup for measuring moisture removal (condensate) and moisture addition through the humidifier. The humidifier is on the scale because it included a small tank that was filled periodically.

The key advantage of this method is that it measures the cumulative moisture removal and addition, instead of measuring the rate. This reduced the uncertainty for this measurement, which was negligible over all time periods of interest. If, instead, we had used flowmeters (one for humidifier supply, one for condensate), the cumulative term (in Eq. (10)) would be the addition of many rate measurements, each with its own uncertainty.

During humidification, the mains-water solenoid valve opened when the mass of the tank/humidifier system dropped below 20 kg, which filled the tank to 30 kg. During dehumidification, the drain solenoid valve would open when the mass of the tank/humidifier system reached 35 kg, and would drain the tank to 25 kg. The humidifier and dehumidifier were turned off during these fill and drain events.

3.1.2 Experimental Validation

A series of preliminary tests were performed to validate the experimental setup. The idea was to link the experiments with an established measurement method. We first linked the new method to an established method with tests in a laboratory chamber (Figure 6). We then linked results using the new method in the field with tests using the new method in the laboratory chamber.

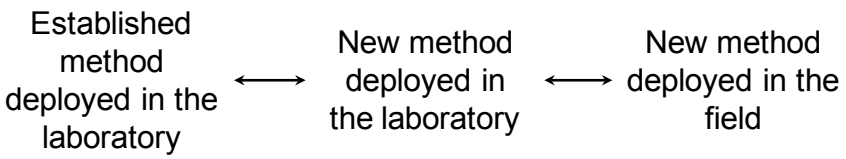

Figure 6. Process used to validate field test method

Linking new method to established method: The initial validation experiments were conducted under a well-controlled environment in an airtight, insulated chamber (Figure 7) in the Advanced HVAC Systems Laboratory at the National Renewable Energy Laboratory. The chamber was constructed with 4-ft × 8-ft sheets of aluminum-faced polyisocyanurate foam board on all six sides. A door was cut in the side for access to the experiment and to change materials, while two windows (cutouts replaced with polycarbonate sheets) allowed visual access during the tests. All edges and seams, including the door and windows, were sealed inside and out with aluminum tape.

The instruments and equipment used in the laboratory chamber test are shown in Tables 3 and 4. There was no dehumidification or cooling equipment in the laboratory chamber. Instead, the temperature of the chamber was kept slightly higher than the laboratory temperature so that no cooling was required. The tests were run as half cycles, without the dehumidification step, which would require cooling because the dehumidifier converts latent energy into sensible energy.

(a)

(b)

Figure 7. Chamber for laboratory-scale testing: (a) exterior, (b) interior

Table 3. List of Measurement Method/Instrumentation for Laboratory Chamber Tests

Measurement	Measurement Method/Instrumentation
Zone humidity	Type-T thermocouples (calibrated to ±0.2°C) Edgetech dew point hygrometer (dew-point ±0.15°C)
Infiltration	Calibrated out using tests with no materials
Moisture addition	Sartorius Signum 35-kg scale (±0.001 kg)
Moisture removal	No air conditioner or dehumidifier
Material sorption	Adam Equipment CBK-16 Scale (±0.001 kg) (and calculated from above measurements)

Table 4. List of Equipment for Laboratory Chamber Test

Humidifier	Humidifirst MP-5
Heater(s)	1500-W electric ceramic heater

The airtightness of the chamber was inferred with several tests on an empty chamber with no moisture sorbent material. This would ideally give a horizontal line through the x-axis in Figure 3(b); any deviation in the y-intercept from zero would likely be due to the moisture buffering capacity of the experimental equipment in the chamber, and any deviation in slope from the x-axis likely to air infiltration. These deviations were measured in 10 empty chamber tests; one test is shown as an example in Figure 8. In this figure, $M_{v,gain}$ is the moisture added to the space from the humidifier and $M_{v,air}$ is the change in moisture in the chamber air (measured as a change in humidity ratio). These nearly balance (i.e., most of the moisture added to the chamber goes to the air). The deviation ($M_{v,(?)}$) is caused by unknown sources, perhaps moisture sorption in material in the chamber, moisture transfer through the chamber walls, or measurement uncertainty. The deviations from the 10 tests were used to correct the results from subsequent chamber tests.

The validation tests in the laboratory chamber used 144 ft^2 of gypsum board. The backside of each sheet of gypsum board was attached to the backside of another, with the edges taped, such that it was exposed on one side only. The established method for measuring moisture sorption into the materials is to weigh the materials directly as they absorb and desorb moisture. Any increase in weight as the RH increases is due to water sorption in the material. Therefore, the moisture absorbed by 16 ft^2 of the total was also measured by weighing it with a second scale. This was extrapolated to the total 144 ft^2, tying the new measurement technique to a well-established method for measuring material moisture sorption.

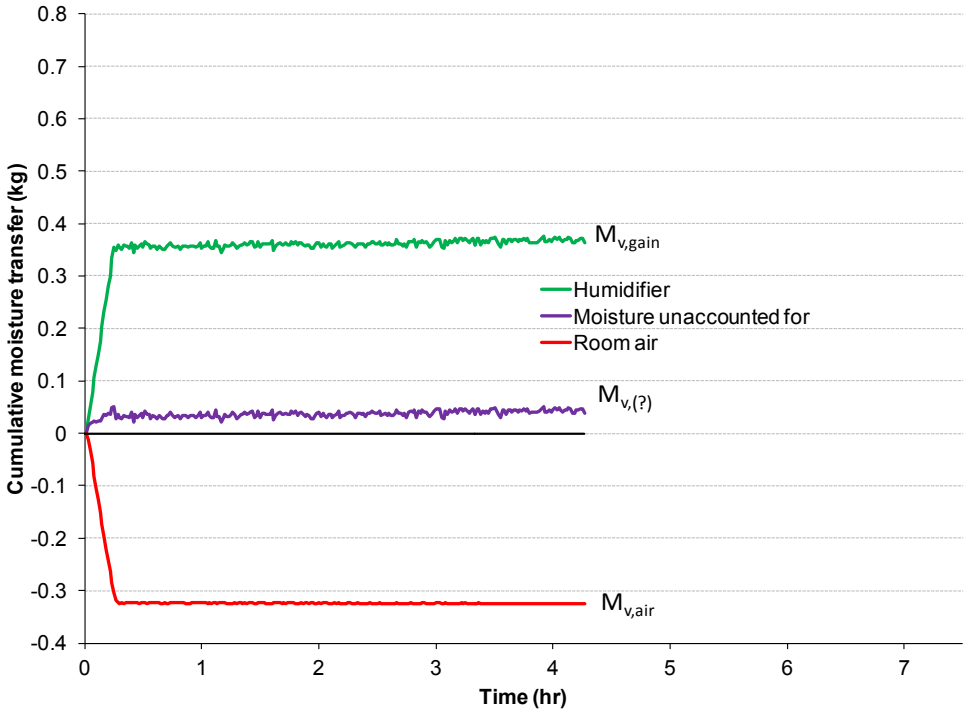

Figure 8. Cumulative moisture transfer during an empty-chamber test in the laboratory

Figure 9 shows the cumulative moisture transferred during this validation test; each of the four lines represents a term in Eq. (10):

- $M_{v,inf}$ is the line just below the x-axis. It is assumed to be infiltration through the chamber, but it accounts for any unknown moisture transfers, which were measured with the 10 tests on an empty chamber (see Figure 8). It is negative because all these 10 tests showed some unknown moisture sink (which is consistent with infiltration from the dry laboratory air into the humid chamber).
- $M_{v,gain}$ is the top line. This is the cumulative moisture added with the humidifier.
- $M_{v,HVAC}$ is zero.
- $M_{v,air}$ is the bottom line. This is the change in mass of the moisture in the chamber air.
- $M_{v,matl}$ is plotted twice. The first is based on Eq. (10) (solid line). The second is based on the established method of directly measuring the change in material weight with time (open circles).

The uncertainty in the established method is due only to the uncertainty in the second scale (±0.001 kg). The uncertainty in the new method (caused by uncertainty in the zone volume, the zone humidity, and the calibrated infiltration) is shown with a single error bar near the 7 hour point. The magnitude of the uncertainty at earlier times was similar.

This comparison shows that the new measurement method results in cumulative moisture transfer nearly equivalent to the established method.

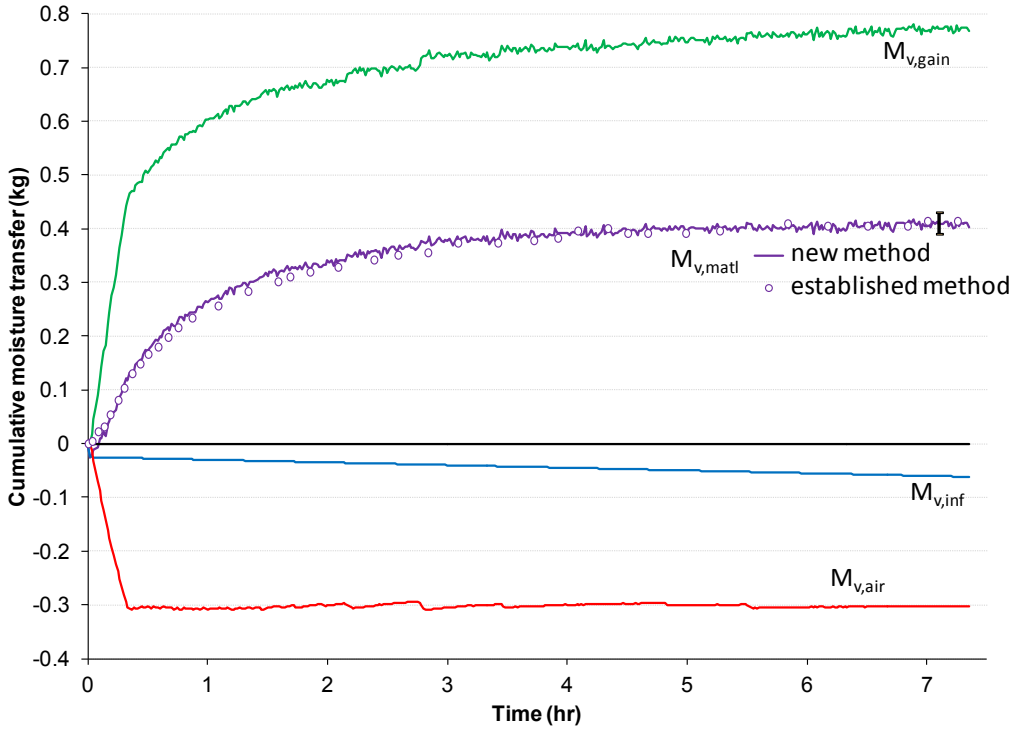

Figure 9. Cumulative moisture transferred into gypsum board in laboratory chamber that is used to validate the experimental method

Linking method in the laboratory with method in the field: The second step of validation was to link the field-test measurements to the laboratory measurements. To do this, we put 2300 ft2 of gypsum board (exposed on both sides) in the field test house and measured its moisture absorption. Before testing the gypsum board, we needed baseline results on an empty house (similar to the baseline tests on the empty chamber). For these tests, we left the exterior walls and ceiling exposed, but covered the bare concrete slab to avoid its expected large moisture capacitance. The house during this configuration is shown in Figure 10; the house with the 2300 ft2 of gypsum board is shown in Figure 11.

We then shipped 48 ft2 of this gypsum board to the laboratory in Colorado and measured it (exposed on both sides) in the chamber. Note that Figure 9 is a moisture transfer plot for one type of gypsum board, which was tested before we received the gypsum board from Florida. A second type (from Florida) was tested in both the field test and the laboratory chamber test.

Figure 10. Field test of empty house with slab covered

Figure 11. Field test of 2300 ft^2 of gypsum board with slab covered

(Photo credit: David Hoak, FSEC. Used with permission.)

Similar to Figure 9, the same four cumulative moisture terms are shown in Figure 12 for the field tests with drywall. Four cycles are shown, each with a humidification and a dehumidification step.

Compared with the laboratory chamber tests, a few differences are worth noting. The Mv,gain line from Figure 9 becomes Mv,gain – Mv,HVAC in Figure 12, with Mv,HVAC representing the

moisture removed both with the dehumidifier and the air conditioner. The dehumidifier is on during the second half of each cycle (12 < t < 24 hours, 36 < t < 48 hours, etc.). The house is not as airtight as the laboratory chamber, so more moisture is transferred through infiltration. The abrupt changes in the slope of the infiltration line every 12 hours is from the changing indoor humidity: during humidification (RH = 65%) the humidity ratio was similar to outdoors; during dehumidification (RH = 35%) the humidity ratio was much lower than outdoors. This infiltration causes the average of the "Mv,gain - Mv,HVAC" line to deviate from the x-axis; there was more dehumidification than humidification to maintain the 35%/65% cycles because of the moisture gained from infiltration. The moisture absorbed by the materials also deviates slightly from the x-axis, but the deviation is much smaller. This deviation was likely due to one (or more) of the following three factors: (1) uncertainty in the infiltration measurement; (2) slow moisture absorption by some of the building materials (likely the concrete block walls); and (3) moisture diffusion through the building envelope, which is not captured in the infiltration measurement.

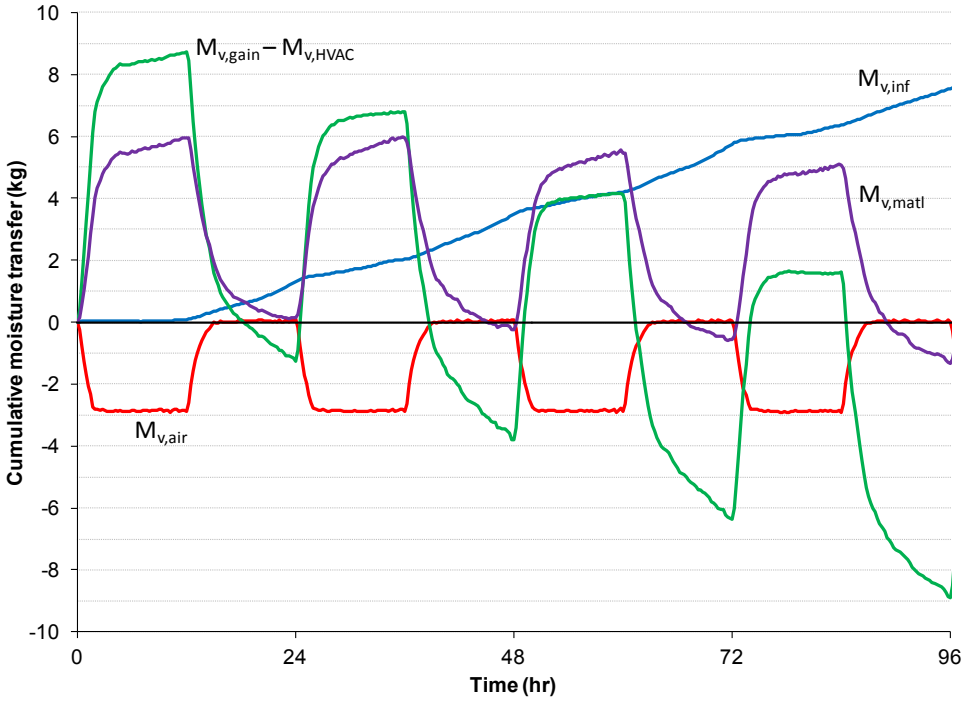

Figure 12. Cumulative moisture transfer for four cycles of whole-house tests with gypsum board

To validate the whole-house test setup, the Mv,matl line in Figure 12 was compared with the Mv,matl line from the laboratory chamber tests. Two corrections to the whole-house test were made before this comparison: (1) The results from the empty-house test were subtracted from the data. This isolates the moisture absorption into the gypsum board (results for the empty house are shown in Figure 17 in Section 4.1); and (2) The material moisture absorption during the humidification steps was averaged with the material moisture desorption during the dehumidification steps.

The moisture sorption curve with these corrections is shown in Figure 13b; the data from the same material measured in the laboratory are shown in Figure 13a. We show the normalized sorption into the materials (kg/m2), because there was more gypsum board in the whole-house

test than in the laboratory chamber test. Two uncertainty bars are shown: one during the ramping RH period, and one during the steady RH period. These are representative of the uncertainties of all the points in each period, but for clarity only one is shown.

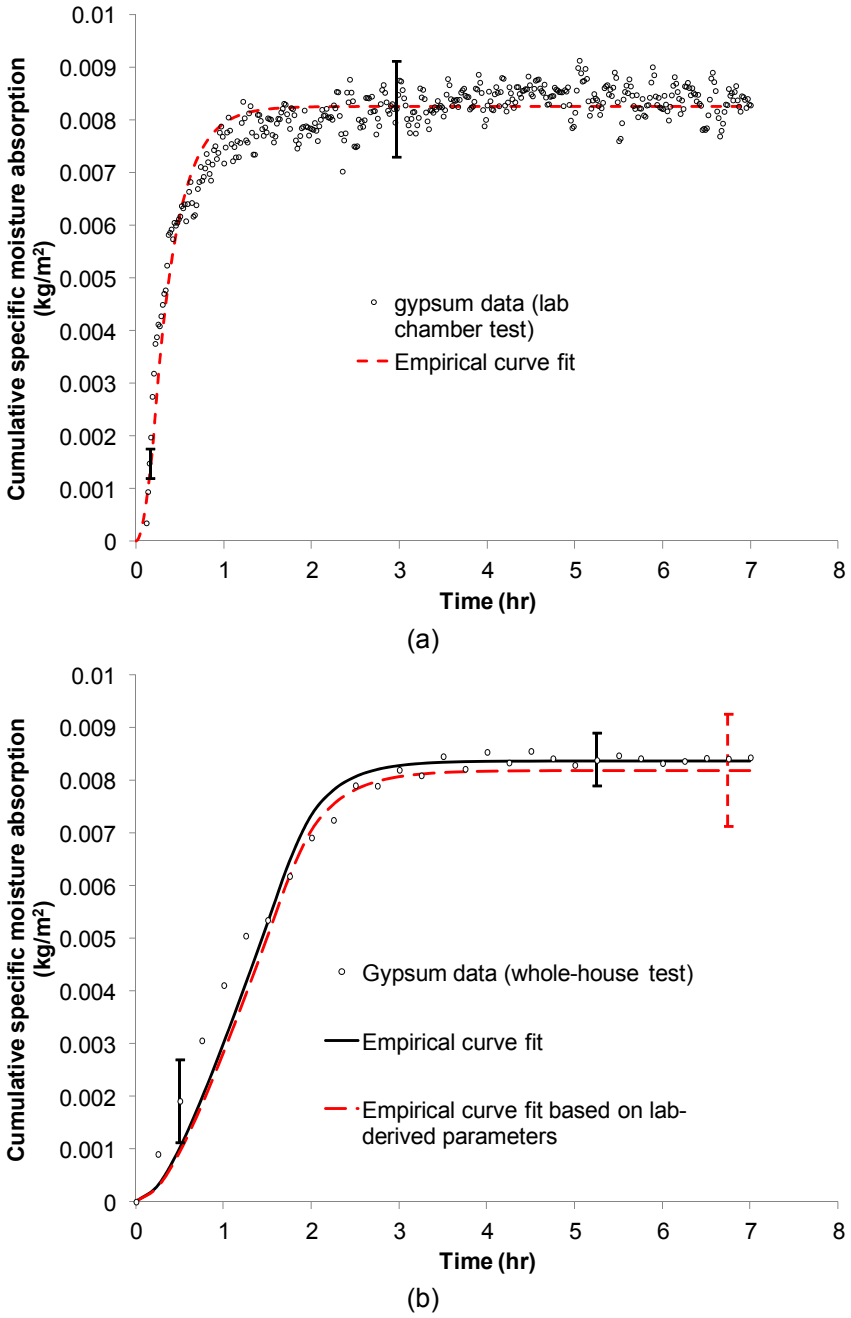

Figure 13. Comparison of tests on gypsum board in (a) laboratory chamber, (b) whole house

From these curves, we see that the RH increases more slowly in the whole-house test than in the laboratory chamber test. This is because the ratio of the humidifier capacity to the moisture capacitance of the air and materials in the space is smaller in the whole-house test. This difference means the results of the two tests cannot be compared directly. Instead, we use our parameter derivation method (see Section 3.2 for an explanation) to compare the results from each test. The red dashed line in Figure 13a is a best-fit line based on Eq. (10); the model parameters are calculated to minimize the sum of the squares of the error between the line and the data. Using the same parameters in Eq. (10), but with the temperature, barometric pressure, and RH data from the whole-house tests, gives the red dashed line in Figure 13b. We also calculated a best-fit line based on the whole-house data, which is the black solid line in Figure 13b. These lines nearly match, with the derived model inputs within 3.5%. This links the measurements in the field to the measurements in the well-controlled laboratory chamber.

3.1.3 Incremental Whole-House Buffering Experiments

With the experimental approach validated, we turn to the incremental moisture buffering tests on the whole house with varying levels of furnishings. From the baseline test with the covered slab, we then measured the incremental moisture buffering effects of: (1) uncovered slab, (2) carpet and pad, (3) furniture, and (4) interior walls.

The vapor barrier was removed from the slab to determine its moisture buffering effect. During the construction of the house, a 6-mil polyethylene vapor barrier was installed below the slab, which minimizes moisture exchange with the soil.

For the carpet tests (Figure 14), we covered the slab with a polyester carpet over a 0.42-in. thick bonded urethane foam pad.

Figure 14. Field test with carpet and pad installed over the slab

(Photo Credit: David Hoak, FSEC. Used with permission.)

For the furniture tests (Figure 15), an assortment of furniture typical for a three-bedroom home was added to the house (without removing the carpet). The furniture included:

- Living and dining room furniture (sofa, chair, throw pillows, end tables, dining table and chairs, rugs)
- Master bedroom (headboard, queen mattress set with linens and pillows, dresser, nightstand)
- Bedroom 2 (headboard, twin mattress set with linens and pillows, dresser, nightstand)
- Bedroom 3 (headboard, twin mattress set with linens and pillows, dresser, nightstand).

For the interior wall tests (Figure 16), the walls were not installed as a floor plan, but instead were built 4-ft tall and 8-ft wide and arranged in two groups of 12 and one group of 11 (total of 2240 ft^2 of interior wall surface area). This provided better mixing and therefore more uniform distribution of temperature and RH. The walls were built uninsulated with 16-in. on-center vertical studs, with the top, bottom and side plates sealed to moisture. The wide sides (gypsum faces) included wooden baseboards. Both baseboards and gypsum board were primed and painted with an eggshell finish, water-based latex paint.

Figure 15. Field test with furniture and carpet

(Photo credit: David Hoak, FSEC. Used with permission.)

Figure 16. Field test with interior walls, furniture, and carpet

(Photo credit: David Hoak, FSEC. Used with permission.)

3.2 Determining Empirical Model Inputs

The $M_{v,matl}$ data obtained from the experiments can be used to derive the EMPD model parameters for this house. We start with the model's moisture balance equations for the surface layer (Eq. (4)). As discussed in Section 2, this equation contains the material moisture content in equilibrium with the zone air (w_{zone}). We use the definition of the material moisture sorption curve to replace this with the sorption curve slope times the zone RH.

$$Ad_{EMPD}\frac{dw_{surf}(t)}{dt} = k_{surf}A\left(\frac{dw}{d\phi}\phi_{zone}(t) - w_{surf}(t)\right) \tag{20}$$

The zone RH is measured, while the sorption curve slope is a new unknown parameter. This is an ordinary differential equation, which is relatively straightforward to solve. To do this, we split the problem into two parts. For the first part, we assume a linearly increasing zone RH (with slope m_r), which is a good approximation for the transient time between the test start and the time when the RH reaches its steady state value. The second part is this steady-state value, where we assume a constant zone RH.

Solving these ordinary differential equations for $w_{SURF}(t)$ results in the following two equations for the transient and steady-state parts (see Appendix for derivation):

$$w_{SURF}(t) = \frac{dw}{d\phi}\left(\phi_{ZONE}(0) - m_r \frac{d_{EMPD}}{k_{surf}} + m_r t \right) + \frac{dw}{d\phi} m_r \frac{d_{EMPD}}{k_{surf}} exp\left(-\frac{k_{surf}}{d_{EMPD}} t \right) \quad 0 < t \le t_1 \tag{21}$$

$$w_{SURF}(t) = \frac{dw}{d\phi}\phi_{ZONE,f} + \left(w_{SURF}(t_1) - \frac{dw}{d\phi}\phi_{ZONE,f} \right) exp\left(-\frac{k_{surf}}{d_{EMPD}}(t - t_1) \right) \quad t > t_1 \tag{22}$$

where t_1 is the time when the period with linearly increasing RH changes to the steady-state period (65% RH). These equations give the moisture content of a uniform layer of fictitious material representing all of the materials in the zone. Combining these with Eqs. (2), (3),and (10), we can calculate the total accumulation of moisture in the materials:

$$M_{v,SURF}(t) = A d_{EMPD} \frac{dw}{d\phi} m_r \left(t - \frac{d_{EMPD}}{k_{surf}} \left[1 - exp\left(\frac{-k_{surf}}{d_{EMPD}} t \right) \right] \right) \quad 0 < t \le t_1 \tag{23}$$

$$M_{v,SURF}(t) = M_{v,SURF}(t_1) + A d_{EMPD} \left(\frac{dw}{d\phi}\phi_{ZONE,f} - w_{SURF}(t_1) \right) \left[1 - exp\left(\frac{-k_{surf}}{d_{EMPD}}(t - t_1) \right) \right] \quad t > t_1 \tag{24}$$

The data from the 2-week tests were used in a similar manner to calculate the deep-layer properties. But the initial ramp was less than 1% of the 2-week test, and can be ignored for deriving the deep-layer properties. The total accumulated moisture during these 2-week tests is accounted for in both the surface and deep layers.

$$M_{v,TOTAL}(t) = M_{v,SURF}(t) + A d_{EMPD-deep} \frac{dw}{d\phi} \left(\phi_{ZONE,f} - \phi_{ZONE,i} \right) \left[1 - exp\left(\frac{-k_{deep}}{d_{EMPD-deep}} t \right) \right] \quad t > 0 \tag{25}$$

The measured data can be compared to Eqs. (23) and (24) for the 24-hour tests, and Eq. (25) for the 2-week tests. We calculate the moisture buffering parameters that minimize the sum of the square of the errors between the data and the model. To do this, we need to know what parameters to solve for. There are several unknowns:

A	material total surface area (m^2)
d_{EMPD}	surface layer EMPD thickness (m)
$d_{EMPD\text{-}deep}$	deep layer EMPD thickness (m)
$dw/d\phi$	moisture sorption curve slope (kg m^{-3} RH^{-1})
k_{surf}	moisture transfer coefficient between air and surface layer (m s^{-1})
k_{deep}	moisture transfer coefficient between surface layer and deep layer (m s^{-1})

However, these variables do not need to be determined independently because many are coupled. There are two groups for the surface layer equations (Eqs. (23) and (24)):

$$\Pi_1 = A d_{EMPD} \frac{dw}{d\phi} \tag{26}$$

$$\Pi_2 = \frac{k_{surf}}{d_{EMPD}} \tag{27}$$

And another two groups in Eq. (25):

$$\Pi_3 = A d_{EMPD-deep} \frac{dw}{d\phi} \tag{28}$$

$$\Pi_4 = \frac{k_{deep}}{d_{EMPD-deep}} \tag{29}$$

These four parameters can be reduced to three. We first use the definition of the deep-layer mass transfer coefficient (Eq. (7)):

$$\Pi_4 = \frac{1}{\frac{d_{EMPD-deep}}{k_{surf}} + \frac{\frac{dw}{d\phi}\left(d_{EMPD-deep}\right)^2 \mu}{2\delta_{air} p_{sat}}} = \frac{1}{\frac{1}{\Pi_2}\frac{d_{EMPD-deep}}{d_{EMPD}} + \frac{1}{\Pi_2}\frac{k_{surf}}{d_{EMPD}}\frac{\frac{dw}{d\phi}\left(d_{EMPD-deep}\right)^2 \mu}{2\delta_{air} p_{sat}}} \tag{30}$$

We then use the definition of the surface-layer mass transfer coefficient (Eq. (6)), along with the fact that $\Pi_3/\Pi_1 = d_{EMPD\text{-}deep}/d_{EMPD}$:

$$\Pi_4 = \frac{1}{\frac{1}{\Pi_2}\frac{\Pi_3}{\Pi_1} + \frac{1}{\Pi_2}\frac{\Pi_3}{\Pi_1} k_{surf} d_{EMPD-deep} \frac{\frac{dw}{d\phi}\mu}{2\delta_{air} p_{sat}} x \frac{d_{EMPD}}{d_{EMPD}}} = \frac{1}{\frac{1}{\Pi_2}\frac{\Pi_3}{\Pi_1} + \frac{1}{\Pi_2}\left(\frac{\Pi_3}{\Pi_1}\right)^2} \tag{31}$$

After some algebra, we end up with a relationship for Π_4 based on the other three Π groupings:

$$\Pi_4 = \frac{\Pi_2 \Pi_1}{\Pi_3\left(1 + \Pi_3/\Pi_1\right)} \tag{32}$$

Thus, three parameters are needed to fully define the EMPD model inputs. In the building energy model, we would like to have realistic material inputs, rather than the empirical Π groupings. We can assume values for some variables and calculate three empirical values. Here, we assume values for $dw/d\phi$, and μ, and then we calculate the total surface area (A), the surface-layer EMPD thickness (d_{EMPD}), and the deep-layer EMPD thickness ($d_{EMPD\text{-}deep}$).

3.3 Realistic Load Test Case

With these empirical parameters calculated, their accuracy was assessed by using them in a model and comparing the model's output with measured data. We use not only the EMPD model, but also the effective capacitance model for comparison. The measured data were taken

from a 24-day test (December 21, 2013 to January 14, 2014), which included enough variation in the weather to provide a reasonable assessment of model accuracy. The heaters and humidifier simulated occupants and internal gains, while the dehumidifier was turned off, and the heaters and air conditioner controlled the zone temperature to between 21.1°C (heating set point) and 25°C (cooling set point). The internal gain profile was based on the Building America House Simulation Protocols [15]. We also added internal gains that mimicked solar gains through windows, because the windows were still covered to prevent condensation. The solar gains through the windows were calculated assuming a relatively clear day and a solar heat gain coefficient of 0.3.

To isolate the moisture buffering model, we simplified the sensible energy calculations by setting the zone temperature in the model equal to the measured value at each time step. This eliminates any uncertainty with the heat transfer model, which is not being evaluated. We also assumed a high mass transfer coefficient at the material surfaces, because the fans operated continuously.

Since we specified the zone temperature in the model, we did not calculate the loads required to maintain the temperature set point. We did, though, need to calculate the moisture removal by the air conditioner, as this impacts the moisture balance. For this, we used the rated air conditioner capacity with an assumed rated sensible heat ratio, and then calculated the latent removal at each time step using the bypass-factor method [16]. We prefer this approach to using the measured latent removal directly, because the modeled latent removal is a function of the zone humidity, and the modeled zone humidity will not, in general, match the measured zone humidity at each time step, especially for the inaccurate EC model.

Other inputs into the model include the ambient humidity ratio, used to calculate the latent infiltration exchange, the barometric pressure, used to calculate various psychrometric functions, and the zone volume.

4 Results and Discussion

4.1 Incremental Whole-House Buffering Tests

The results of the whole-house incremental tests are shown in Figures 17 and 18 for the 24-hour tests and 2-week tests, respectively. They show the results for each level of materials. We averaged the material absorption during the humidification steps with the material desorption during the dehumidification steps to obtain the curves shown in the figures. This averaging forces the line to return to zero at the end of the dehumidification step. For clarity, these plots do not include uncertainty bars; the uncertainty of these experiments is discussed in Section 4.2.

Twenty-four-hour tests (Figure 17): The first case for the 24-hour tests is an empty house, which includes the buffering effects of the exterior walls and the ceiling. Temperature and RH sensors between the gypsum board and the concrete blocks of the exterior walls indicated that the moisture penetrated the gypsum board and was absorbed by the concrete blocks. Thus, the blocks are responsible for at least part of the absorption seen in the empty house test.

After the empty house test, we incrementally looked at the effects of various materials in the space. The vapor barrier was removed from the floor so that the concrete slab would absorb moisture. This nearly doubled the moisture absorption from the empty house test, with 3.7 kg of

moisture being absorbed. Adding carpet gives the next line, which shows that carpet absorbs moisture quickly, based on the faster absorption of the carpet compared to the bare slab for the first 3 hours. However, the carpet slows the moisture absorption into the slab, so that at the end of the humidification step, the bare slab was absorbing moisture more quickly than the slab with carpet. Adding carpet increased the cumulative absorption over 12 hours by 0.5 kg. The next two steps (adding furniture and then interior walls) each increased the moisture absorption by roughly 1.7 kg.

The total moisture absorbed (7.6 kg) for the final case is roughly 2.7 times higher than the change in moisture in the zone air. This final case is used in Section 4.3 to derive the overall buffering properties of the house.

Two-week tests (Figure 18): The 2-week tests started with a dehumidification step. We again averaged the measured moisture desorption during dehumidification and the measured absorption during humidification. For the final test (interior walls + furniture + carpet), the materials absorbed 37 kg of moisture. This is 13 times higher than the change in moisture in the zone air. This final test is used to derive the third lumped parameter for the moisture buffering model (Eq. (25)), as discussed in Section 4.3.

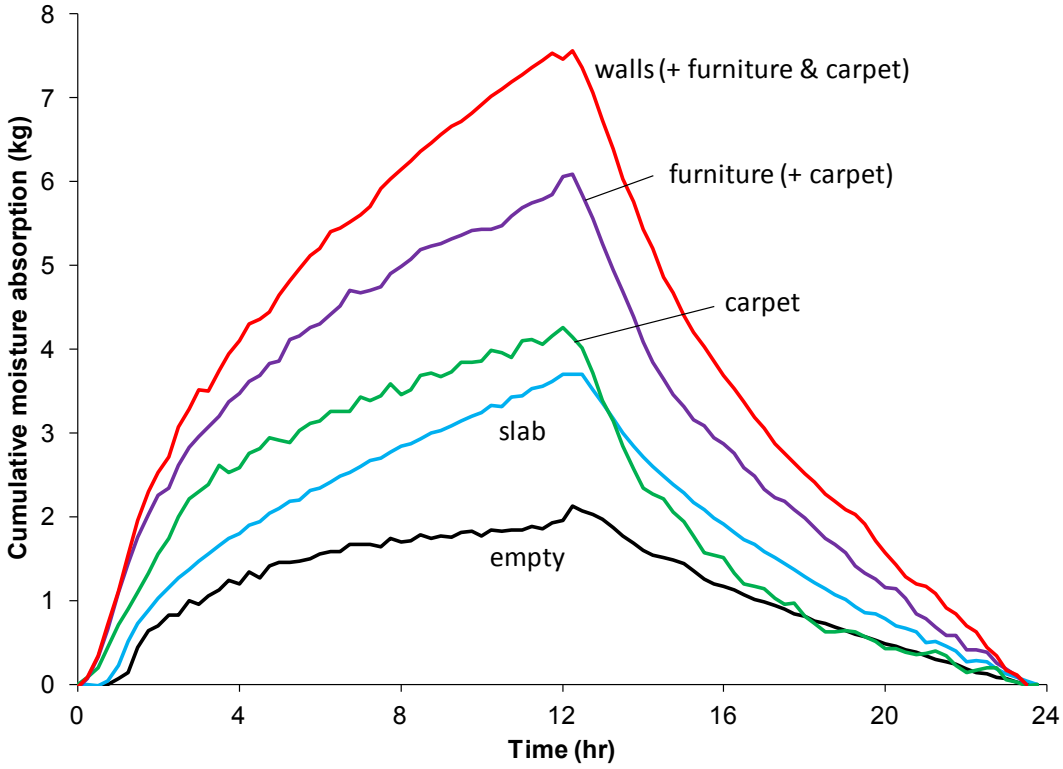

Figure 17. Cumulative moisture sorption for 24-hour cycle tests

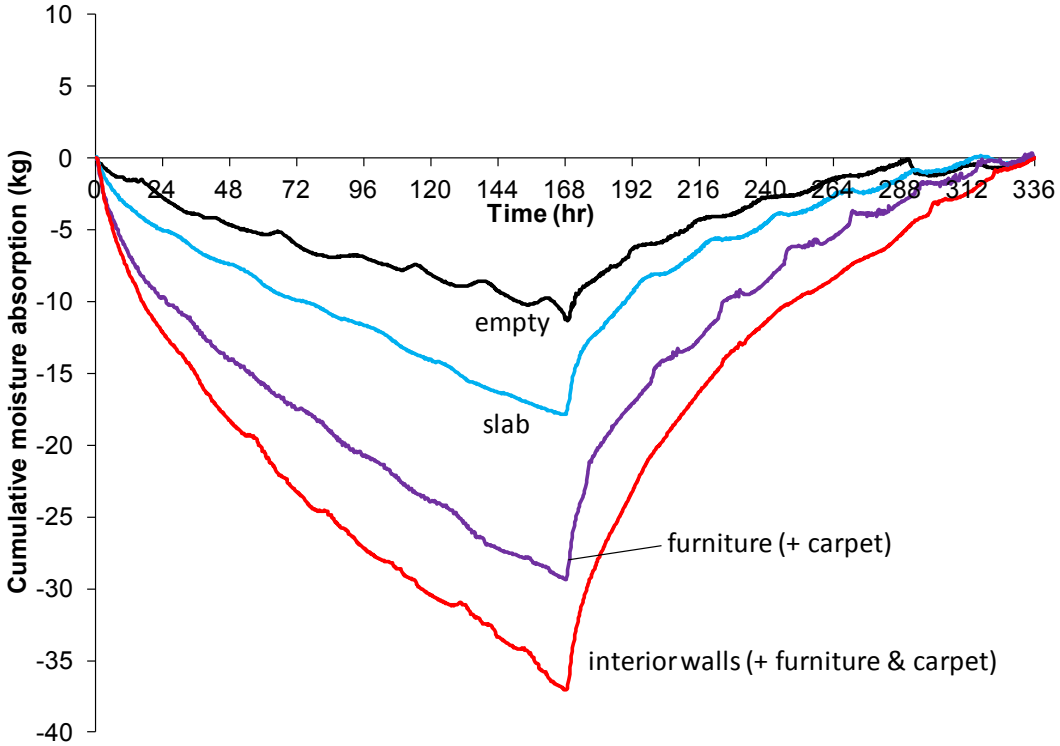

Figure 18. Cumulative moisture sorption for 2-week cycle tests

4.2 Uncertainty Analysis

To improve the readability of the figures, we omitted uncertainty bars from most of the previous graphs. Instead, we show the percent uncertainty versus time for these measurements in Figure 19. The uncertainty is split into two cases: (1) the uncertainty when the ambient humidity ratio is close to the indoor humidity ratio; and (2) the uncertainty when the ambient humidity ratio and indoor humidity ratio differ significantly. Case (1) is typical of a humidification step (when the indoor humidity is high); case (2) is typical of a dehumidification step (when the indoor humidity is low). The actual cases plotted in Figure 19 are: (1) the humidification step of the 2-week tests with a fully furnished house; and (2) the dehumidification step during the 2-week tests with furniture and carpet.

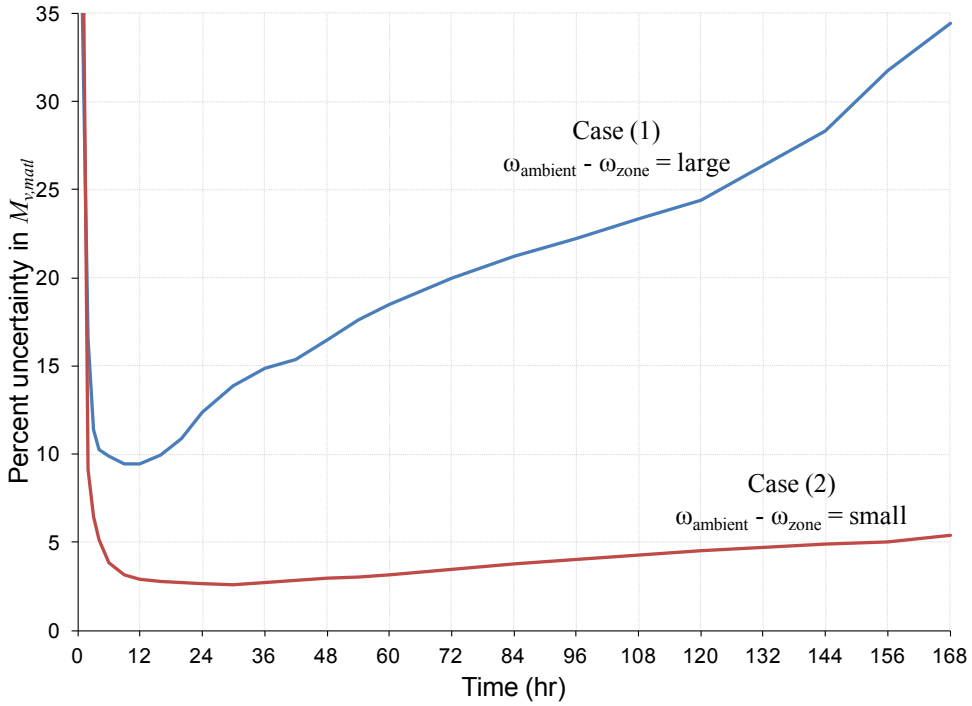

Figure 19. Percent uncertainty in the calculated material moisture sorption

The percentage uncertainty during the first hour is high in both cases. This is partially due to the slightly higher absolute uncertainty during the beginning of these tests, but more due to the lower absolute material absorption during the beginning of the tests, leading to high percent uncertainty. At around 12 hours, a key time for data analysis for the 24-hour tests, the uncertainty is less than 3% for case (1) and 9% for case (2). The uncertainty is around 5% for case (1) for time periods at one week (important for the 2-week test). For case (2), the uncertainty at one week approaches 35%, which is primarily due to the uncertainty in the measurement of the infiltration moisture.

This is illustrated in Figures 20 and 21, which show the apportionment of the overall uncertainty for cases (1) and (2), respectively, to each individual measurement uncertainty.

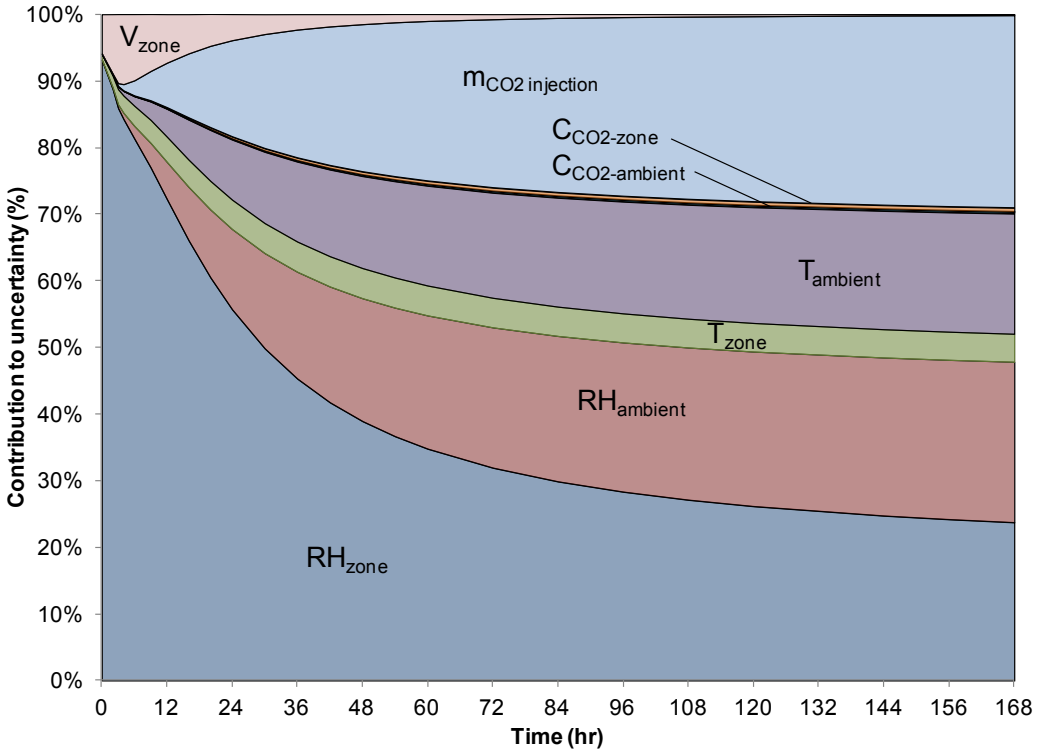

Figure 20. Percent contribution of each measurement uncertainty to the overall uncertainty in the calculated material sorption. Case (1): slight difference between zone and ambient humidity ratio.

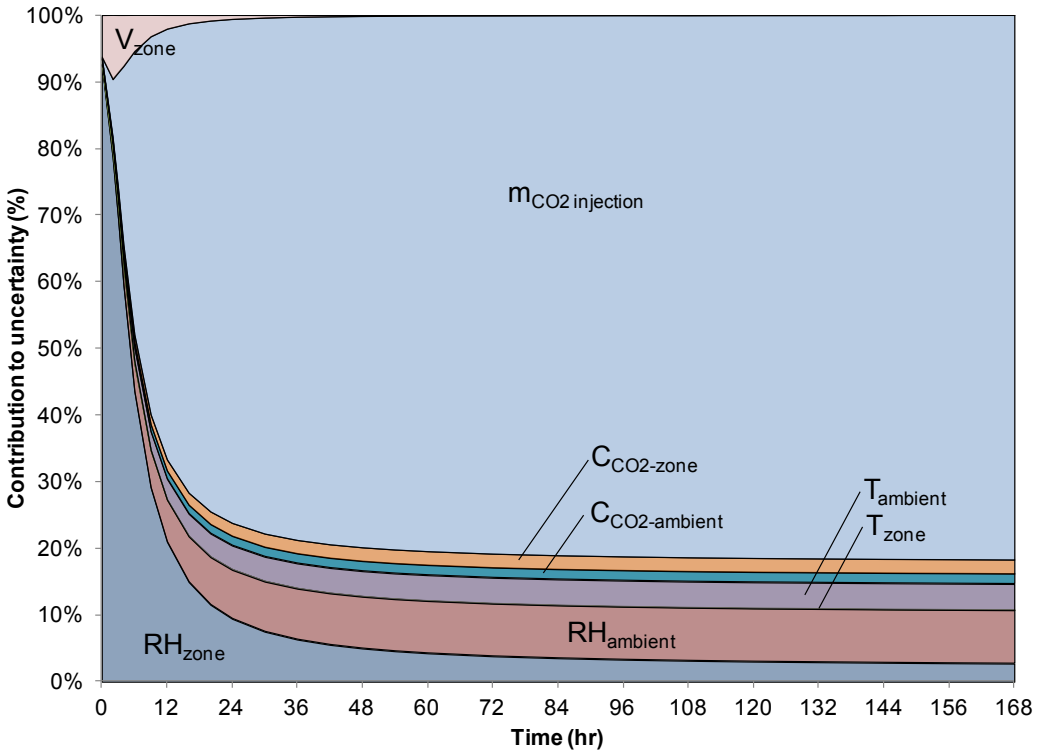

Figure 21. Percent contribution of each measurement uncertainty to the overall uncertainty in the calculated material sorption. Case (2): large difference between zone and ambient humidity ratio.

For case (1), the uncertainty for the initial day is driven by the zone RH measurement. For longer periods, the uncertainty in the infiltration starts to dominate, which is due to both the uncertainty in the humidity ratio difference between the zone and ambient, as well as the infiltration rate ($\dot{m}_{air,inf}$). For case (2), the uncertainty in the tracer gas measurements (primarily the CO_2 injection rate) contribute to nearly 80% of the overall uncertainty after only 24 hours. Since the humidity ratio difference between the zone and the ambient is large, the uncertainty in the actual infiltration rate is more important than for case (1). These results show that uncertainty could be reduced by using a more accurate mass flowmeter. Because this instrument's uncertainty is a percentage of full scale, it could be improved by simply using a smaller mass flowmeter and measuring closer to the upper end of the instrument range.

The uncertainty data are carried through to the overall uncertainty in the empirically derived parameters. These are presented with the parameter values in Section 4.3.

4.3 Empirical Parameter Derivation

The $M_{v,matl}$ data for the 24-hour and 2-week tests can be used to derive the parameters for use in building energy models. The data for these two tests are shown again in Figures 22 and 23, along with the least-squares fit based on Eq. (23) for Figure 22 and Eq. (25) for Figure 23.

The parameters for these least-squares fit curves are shown in Tables 5 and 6. The moisture buffering of the house is fully characterized with any three of these parameters, which can be used as inputs in building simulations. For Table 6, we assume values for the vapor resistance factor and the slope of the sorption curve. These values are arbitrary, because it is the overall groupings that are important, but using these values (typical of gypsum and wood-based materials) give meaningful numbers to the area and penetration depths.

Table 5. Empirically Derived Parameters (Π Groupings)

Π_1 (kg m^{-3} RH^{-1})	Π_2 (s^{-1})	Π_3 (kg m^{-3} RH^{-1})	Π_4 (s^{-1})
31.0 ± 0.414	4.27E-05 ± 0.31E-05	183 ± 34	1.05E-06 ± 0.276E-06

Table 6: Example of Empirically Derived Material Properties

μ	$dw/d\phi$ (kg m^{-3})	A (m^2)	d_{EMPD} (m)	$d_{EMPD\text{-}deep}$ (m)
8.0 †	10.0 †	161.8 ± 8.0	0.0191 ± 0.0007	0.113 ± 0.016

† assumed

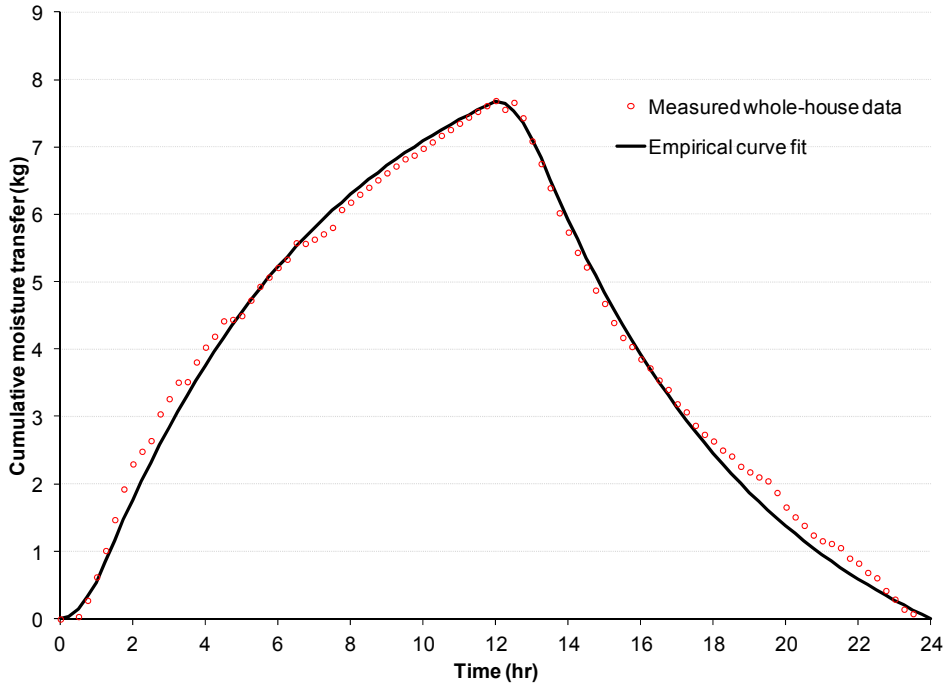

Figure 22. Empirical fit for 24-hour data for all materials in whole-house test

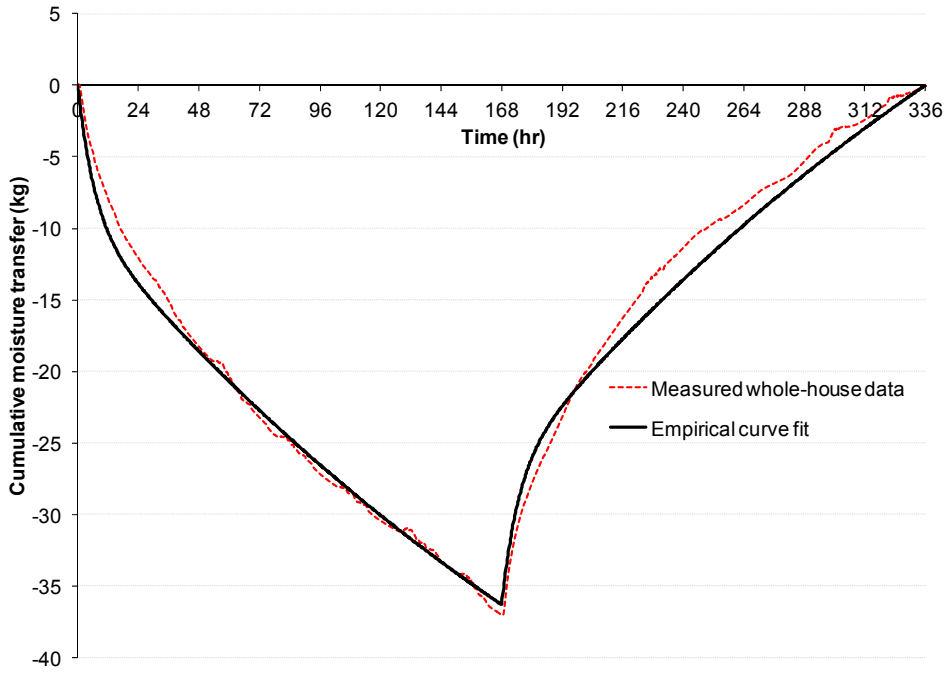

Figure 23. Empirical fit for 2-week data for all materials in whole-house test

4.4 Using the Calibrated Model

The realistic-load test case is used to validate the model and its inputs. The ambient conditions during this test varied as shown in Figure 24. During the cooler periods (hour 315 to 340 and hour 405 to 440), the air conditioner was off for several days. This affects the RH, because the air conditioner is the primary means of removing moisture from the zone.

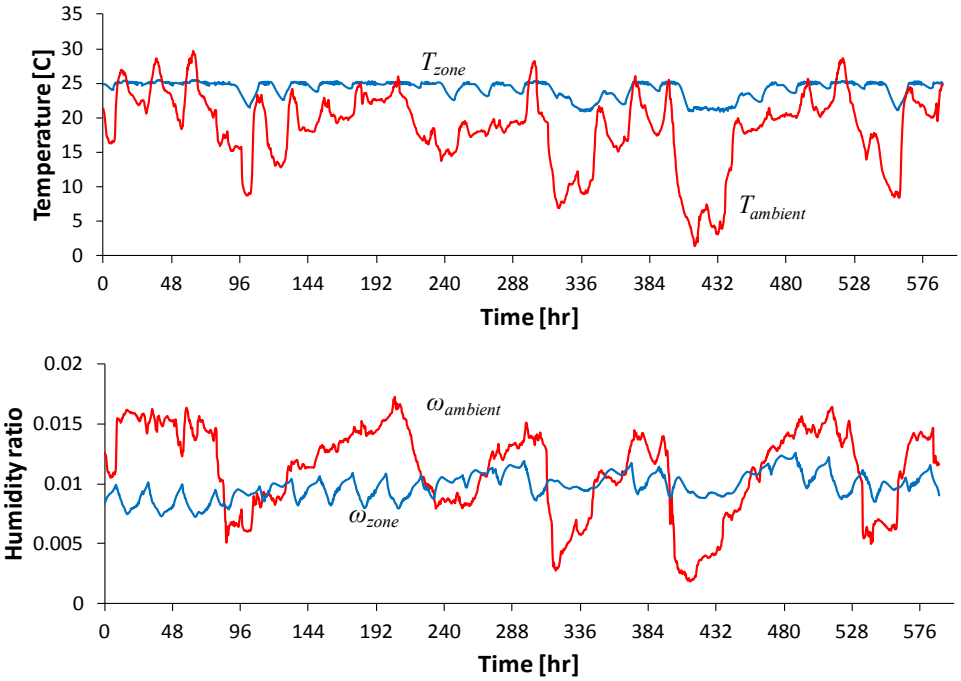

Figure 24. Measured temperature and humidity ratio for the building zone and ambient air during the realistic-load test case

To assess model accuracy, we compare the measured and modeled RH. This is shown in Figure 25 for the EMPD model, Figure 26 for the EC model, and Figure 27 for the EMPD model with no deep layer. The uncertainties for these plots are: 1.7% RH (measured), 0.73% RH (EMPD model), 0.65% RH (EC model), and 0.71% (EMPD model with no deep layer). The uncertainty for the EC model assumes there is no uncertainty in the actual EC value, since this is simply prescribed, but Figure 26 shows the sensitivity to this value with results for EC = 3 and EC = 10.

These figures illustrate how the EMPD model, when using a deep layer, matches the data fairly well, while the EC model does not. The coefficient of determination (R^2), a way to quantify the model accuracy, is $R^2 = 0.81 \pm 0.03$ for the EMPD model with a deep layer. Table 7 shows this value compared to the EC model, which has a maximum R^2 of 0.52 (EC = 5). This shows that the EC model, regardless of what EC value is used, cannot be calibrated; it is incapable of matching the measured data.

The reasons for this can be seen in Figure 26. Using EC = 10 results in overdamping of the daily fluctuations in RH. Using EC = 3 is better for these high-frequency fluctuations, but it results in underdamping of the lower frequency moisture loads (288 hours < t < 480 hours).

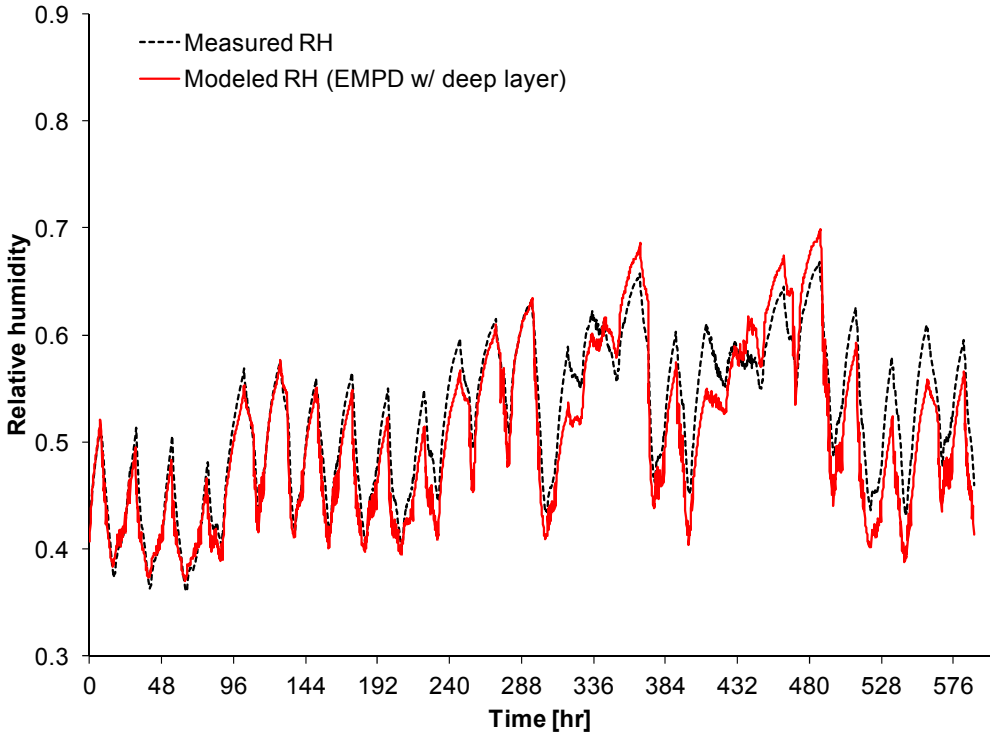

Figure 25. Model-predicted RH for the EMPD model compared to the measured RH during the realistic-load test case

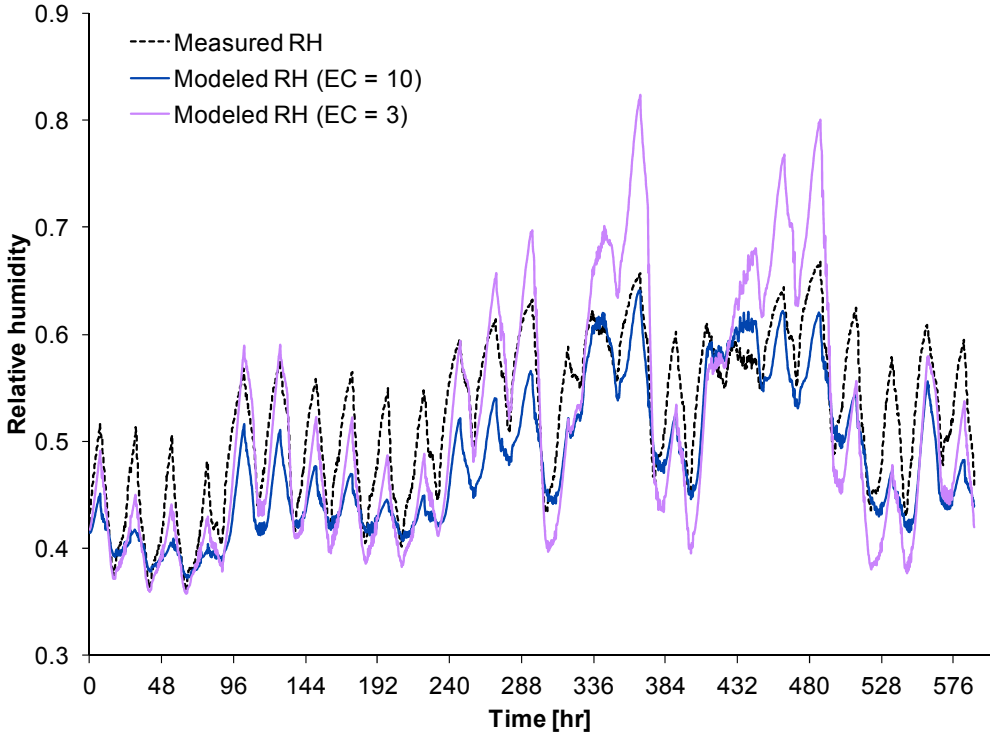

Figure 26. Model-predicted RH for the EC model, with EC = 3 and EC = 10, compared to the measured RH during the realistic-load test case

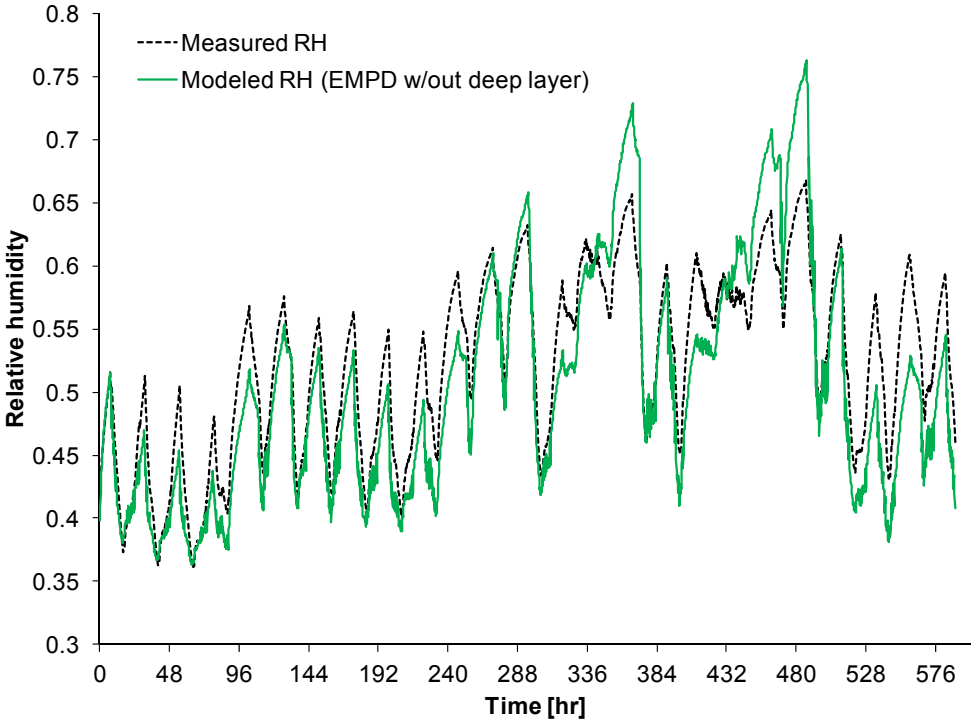

Figure 27. Model-predicted RH for the EMPD model without a deep layer, compared to the measured RH during the realistic-load test case

Table 7. Coefficient of Determination (R^2) for the Model Based on the Realistic-Load Test Case; Uncertainty for EMPD Model Is ±0.03

Model	R^2
EMPD	0.81
EMPD (no deep layer)	0.64
EC = 3	0.29
EC = 5	0.52
EC = 8	0.46
EC = 10	0.40
EC = 15	0.26

The EMPD model with only the surface layer also underdamps the lower frequency moisture loads, but it has a better R^2 (0.64) than the EC model. These results indicate that, at least for houses with similar construction to that tested here, a deep layer is required for an accurate model.

The low uncertainty in the RH predicted by the EMPD model, despite the sizable uncertainties discussed in Section 4.2, indicates that the EMPD model is insensitive to small changes in its inputs. But what about larger changes? We were careful to eliminate uncertainties in the experiments, such as using an accurate scale for measuring moisture addition and removal, minimizing infiltration, and keeping the air conditioner ducts in conditioned space. If we introduced more uncertainty, how would that affect our final "calibrated" model? To explore this

question, we looked at the sensitivity of the final R^2 value to larger uncertainties of the determined parameters (A, d_{EMPD}, and $d_{EMPD\text{-}deep}$). There are only three independent parameters, so looking at the uncertainty of other parameters (e.g., sorption curve) is not meaningful. This does not answer this question definitively, because we have only 3.5 weeks of monitored data on just one house. But it gives a good initial assessment of the sensitivity of the model to its inputs.

To calculate the sensitivity, we changed the values of the three inputs by 10 standard deviations in both directions (±25% for A, ±20% for d_{EMPD}, and ±70% for $d_{EMPD\text{-}deep}$) and calculated the change in R^2. The largest change (Table 8) is from $R^2 = 0.81$ to $R^2 = 0.74$ for a 25% smaller material surface area.

The effect of the deep layer thickness changing by ±70% has little effect on R^2. So the deep layer is important (eliminating the deep layer reduces R^2 from 0.81 to 0.64), but the value for the deep layer thickness is less important.

Table 8. Sensitivity of Results to a 10-Standard-Deviation Change in Each Input Parameter

Case	R^2
Baseline	0.81
1.25A	0.79
0.75A	0.74
1.2d_{EMPD}	0.83
0.8d_{EMPD}	0.77
1.7$d_{EMPD\text{-}deep}$	0.78
0.3$d_{EMPD\text{-}deep}$	0.81

This shows that the model is relatively insensitive to the accuracy of these inputs. Although estimating the values based solely on house characteristics, which may provide an order of magnitude estimate, is still not an option, it may allow for less rigorous measurement techniques without much sacrifice in accuracy. It also means a limited dataset, based on tests on a handful of houses, may be adequate to develop correlations for the model inputs based on house size, construction materials, and level of furnishings.

5 Conclusions

This study validated a method for calculating material moisture sorption by measuring all other moisture transport terms during well-defined RH cycles. This allows us to derive moisture model inputs for building simulations by testing houses in the field. The results of the house tested in this study showed that using these derived model inputs in a building simulation accurately predicted the RH in the house during a test under Building America operation protocols.

The EMPD model can be fully defined with three independent parameters that are groups of material properties and geometric inputs. By assuming values for the material properties, we can obtain more intuitive inputs: the surface area of the material, the surface-layer thickness, and the deep-layer thickness.

The method is less accurate over longer time periods, but the model was still accurate for two reasons: (1) the first two model parameters were derived based on data over short periods; and (2) the model is relatively insensitive to the third parameter, which is derived based on data over longer periods. The key driver in the accuracy was the uncertainty in the infiltration measurement; improving this measurement would provide the largest reduction in uncertainty.

That being said, the final modeling results were relatively unaffected by these uncertainties. This means simpler measurement techniques may be possible without sacrificing accuracy. For example, a simple model of infiltration, based on a one-time infiltration measurement, could be used instead of continuously monitoring infiltration. These questions require further analysis to understand its importance for different house characteristics (e.g., for leakier houses than the 2.5-ACH50 house used here).

This study provided data for just one house construction, and a few levels of furnishings. This method could be used in houses of other constructions (e.g., wood frame), to determine how the moisture buffering of these homes differ. Several tests could be used to develop a dataset to provide guidance on moisture buffering model inputs for different home constructions and level of furnishings.

Some questions were not addressed in this study, and may need further research:

- How humidity distribution from room to room affects the measurement.
- How sensitive the results are to varying degrees of air conditioner duct leakage.
- The accuracy of the method when measuring air conditioner condensate with a less accurate measurement, such as a tipping bucket. This may be required in cases using the home's existing air handler.

References

[1] Woods, J., J. Winkler, D. Christensen, Moisture modeling: Effective moisture penetration depth versus effective capacitance, in *Thermal Performance of the Exterior Envelopes of Whole Buildings XII International Conference*. 2013: Clearwater, FL.

[2] Rudd, A. and H. Henderson, Monitored indoor moisture and temperature conditions in humid-climate US residences, ASHRAE Transactions. 113 (2007) 435-49.

[3] Henderson, H., D. Shirey, C.K. Rice, Can conventional cooling equipment meet dehumidification needs for houses in humid climates?, in *2008 ACEEE Summer Study on Energy Efficiency in Buildings*. 2008: Pacific Grove, CA.

[4] Kuenzel, H.M., A. Karagiozis, A. Holm, WUFI ORNL/IBP A Hygrothermal Design Tool for Architects and Engineers. 2001, Chapter ASTM Manual 40 in Moisture Analysis of Buildings.

[5] Combined Heat and Moisture Transfer (HAMT) Model, EnergyPlus Engineering Reference. 2013, US Department of Energy. p. 47-52.

[6] Keresteciogl u, A., M. Swami, A. Kamel, Theoretical and computational investigation of simultaneous heat and moisture transfer in buildings: "Effective penetration depth" theory, ASHRAE Transactions. 96 (1990) 447-54.

[7] Cunningham, M.J., Effective penetration depth and effective resistance in moisture transfer, Build. Environ. 27 (1992) 379-86.

[8] Cunningham, M.J., The moisture performance of framed structures - a mathematical model, Build. Environ. 23 (1988) 123-35.

[9] Woods, J., J. Winkler, D. Christensen, Evaluation of the effective moisture penetration depth (EMPD) model for estimating moisture buffering in buildings. National Renewable Energy Laboratory, TP-5500-57441, 2013.

[10] Janssen, H. and S. Roels, Qualitative and quantitative assessment of interior moisture buffering by enclosures, Energ. Buildings. 41 (2009) 382-94.

[11] Abadie, M.O. and K.C. Mendonca, Moisture performance of building materials: From material characterization to building simulation using the Moisture Buffer Value concept, Build. Environ. 44 (2009) 388-401.

[12] Rode, C. and K. Grau, Moisture buffering and its consequence in whole building hygrothermal modeling, Journal of Building Physics. 31 (2008) 333-60.

[13] Vereecken, E., S. Roels, H. Janssen, In situ determination of the moisture buffer potential of room enclosures, Journal of Building Physics. 34 (2011) 223-46.

[14] Vieira, R. and J. Sherwin, Flexible Residential Test Facility Instrumentation Plan. Flordia Solar Energy Center for DOE Building America Program, 2011.

[15] Hendron, R. and C. Engebrecht, Building America House Simulation Protocols. National Renewable Energy Laboratory, TP-5500-49426, 2010.

[16] Threlkeld, J.L., Cooling and Dehumidying Coils, in Thermal Environmental Engineering. 1970, Prentice-Hall: Englewood Cliffs. p. 254-70.

Appendix

This appendix derives the equations used to calculate the material's moisture properties for the surface layer (Eqs. (23-24) and the deep layer (Eq. (25)).

Surface-layer properties: The surface layer equations are derived from the differential equation based on a mass balance for the surface layer:

$$Ad_{EMPD}\frac{dw_{surf}(t)}{dt} = k_{surf}A\left(\frac{dw}{d\phi}\phi_{zone}(t) - w_{surf}(t)\right) \quad (A.1)$$

We start by converting this to the standard format for a first order, linear differential equation:

$$\frac{dw_{surf}}{dt} + p(t)w_{surf} = q(t) \quad (A.2)$$

Where

$$p(t) = \frac{k_{surf}}{d_{EMPD}} \quad (A.3)$$

$$q(t) = \frac{k_{surf}\dfrac{dw}{d\phi}}{d_{EMPD}}\phi_{zone}(t) \quad (A.4)$$

We assume the material properties are constant with time. The solution to this equation is:

$$w_{surf}(t) = \frac{\int_0^t q(t)exp(pt)dt + C}{exp(pt)} \quad (A.5)$$

At this point, we split the problem into two parts: the ramping period and the steady-state period.

Ramping period: During the ramping period, the zone RH is:

$$\phi_{ZONE}(t) = \phi_{ZONE}(0) + m_r t \quad (A.6)$$

where m_r is the rate of increase in the zone RH during this period, which is approximately constant with time, but can differ from one test to the next:

$$m_r = \frac{\Delta\phi}{\Delta t} = \frac{\phi_{ZONE,f} - \phi_{ZONE}(0)}{t_1 - 0} \quad (A.7)$$

where t_1 is the time at which the RH equals its steady-state value. For this period, Eq. (A.5) becomes:

$$w_{SURF}(t) = \frac{\int_0^t \alpha(\phi_{ZONE}(0) + m_r t)\exp(pt)dt + C}{\exp(pt)} \tag{A.8}$$

where α is:

$$\alpha = \frac{k_{surf}\dfrac{dw}{d\phi}}{d_{EMPD}} \tag{A.9}$$

Solving the integral leads to:

$$w_{SURF}(t) = \frac{\alpha}{p}\left(\phi_{ZONE}(0) - \frac{m_r}{p} + m_r t\right) + \left[\frac{\alpha}{p}\left(-\phi_{ZONE}(0) + \frac{m_r}{p}\right) + C\right]\exp(-pt) \tag{A.10}$$

Substituting in the equations for α and p gives:

$$\begin{aligned} w_{SURF}(t) &= \frac{dw}{d\phi}\left(\phi_{ZONE}(0) - \frac{m_r d_{EMPD}}{k} + m_r t\right) + \\ &\left[\frac{dw}{d\phi}\left(-\phi_{ZONE}(0) + \frac{m_r d_{EMPD}}{k_{surf}}\right) + C\right]\exp\left(-\frac{k_{surf}}{d_{EMPD}}t\right) \end{aligned} \tag{A.11}$$

The initial condition $\left(w_{SURF}(0) = \dfrac{dw}{d\phi}\phi_{ZONE}(0)\right)$ is used to solve for C, which gives the surface moisture content during the ramping period:

$$w_{SURF}(t) = \frac{dw}{d\phi}\left(\phi_{ZONE}(0) - m_r\frac{d_{EMPD}}{k_{surf}} + m_r t\right) + \frac{dw}{d\phi}m_r\frac{d_{EMPD}}{k_{surf}}\exp\left(-\frac{k_{surf}}{d_{EMPD}}t\right) \quad 0 < t \le t_1 \tag{A.12}$$

This is converted to the cumulative moisture transfer with:

$$M_{v,SURF}(t) = \int_0^t \dot{m}_{v,SURF}dt = \int_0^t k_{surf}A\left(\frac{dw}{d\phi}\phi_{ZONE}(t) - w_{SURF}(t)\right)dt \quad 0 < t \le t_1 \tag{A.13}$$

where $\dot{m}_{SURF}(t)$ is the instantaneous moisture transfer rate. Substituting Eq. (A.12) for w_{SURF} and (A.6) for $\phi_{ZONE}(t)$ and simplifying gives:

$$M_{v,SURF}(t) = \int_0^t Ad_{EMPD}\frac{dw}{d\phi}m_r\left(1 - \exp\left(-\frac{k_{surf}}{d_{EMPD}}t\right)\right)dt \quad 0 < t \le t_1 \tag{A.14}$$

Integrating leads to the final equation for the cumulative moisture transfer during the ramping period (Eq. (23) in the report):

$$M_{v,SURF}(t) = Ad_{EMPD}\frac{dw}{d\phi}m_r\left(t - \frac{d_{EMPD}}{k_{surf}}\left[1 - exp\left(\frac{-k_{surf}}{d_{EMPD}}t\right)\right]\right) \quad 0 < t \le t_1 \tag{A.15}$$

Steady-state period: During the steady-state period, the zone RH is constant at its final value $\phi_{ZONE,f}$. Eq. (A.5) becomes:

$$w_{SURF}(t) = \frac{\int_{t_1}^{t} \alpha\phi_{ZONE,f}\, exp(pt)dt + C}{exp(pt)} \tag{A.16}$$

Solving the integral leads to:

$$w_{SURF}(t) = \frac{\alpha}{p}\phi_{ZONE,f} - \frac{\alpha}{p}\phi_{ZONE,f}\, exp(-p(t-t_1)) + C\, exp(-pt) \tag{A.17}$$

In this case, the initial condition is $w_{SURF}(t_1)$, which is calculated from the ramping period equation for $t = t_1$. This gives $C = w_{SURF}(t_1)$, and the surface moisture content during the steady-state period becomes:

$$w_{SURF}(t) = \frac{dw}{d\phi}\phi_{ZONE,f} + \left(w_{SURF}(t_1) - \frac{dw}{d\phi}\phi_{ZONE,f}\right)exp\left(-\frac{k_{surf}}{d_{EMPD}}(t-t_1)\right) \quad t > t_1 \tag{A.18}$$

This is converted to the cumulative moisture transfer by adding the total cumulative moisture transfer during the steady-state period (after time t_1) to the cumulative moisture transfer at the end of the ramp period:

$$M_{v,SURF}(t) = M_{v,SURF}(t_1) + \int_{t_1}^{t} k_{surf} A\left(\frac{dw}{d\phi}\phi_{ZONE}(t) - w_{SURF}(t)\right)dt \tag{A.19}$$

Substituting in Eq. (A.18) for $w_{surf}(t)$ and $\phi_{ZONE,f}$ for $\phi_{ZONE}(t)$, and simplifying leads to:

$$M_{v,SURF}(t) = M_{v,SURF}(t_1) + \int_{t_1}^{t} k_{surf} Ad_{EMPD}\left(\frac{dw}{d\phi}\phi_{ZONE,f} - w_{SURF}(t_1)\right)exp\left(-\frac{k_{surf}}{d_{EMPD}}(t-t_1)\right)dt \tag{A.20}$$

Evaluating the integral from t_1 to t gives the final equation for the cumulative moisture transfer to the surface layer for the steady-state period:

$$M_{v,SURF}(t) = M_{v,SURF}(t_1) + Ad_{EMPD}\left(\frac{dw}{d\phi}\phi_{ZONE,f} - w_{SURF}(t_1)\right)\left[1 - exp\left(\frac{-k_{surf}}{d_{EMPD}}(t - t_1)\right)\right] \quad t > t_1 \quad \text{(A.21)}$$

Deep-layer properties: The deep-layer properties are derived based on a moisture balance on the deep layer:

$$Ad_{EMPD-deep}\frac{dw_{deep}(t)}{dt} = k_{deep}A\left(w_{surf}(t) - w_{deep}(t)\right) \quad \text{(A.22)}$$

which can be rearranged to:

$$\frac{dw_{deep}(t)}{dt} + \frac{k_{deep}}{d_{EMPD-deep}}w_{deep}(t) = \frac{k_{deep}}{d_{EMPD-deep}}w_{surf}(t) \quad \text{(A.23)}$$

Again, Eq. (A.5) is the solution to this differential equation. At this point, we simplify the equation by assuming that the surface layer absorbs moisture much more quickly than the deep layer. We have assured this to be true based on the definitions of the surface and deep layers: the surface layer becomes saturated after 12 hours; the deep layer becomes saturated after 168 hours. In other words, the resistance and capacitance of the surface layer affect only the first 7% of the absorption period for the deep layer. This has a minimal impact on our data analysis method (see Figure 23). Based on similar arguments, we also assume that the ramping period is negligible for the deep layer. These assumptions lead to:

$$\frac{dw_{deep}(t)}{dt} + \frac{k_{deep}}{d_{EMPD-deep}}w_{deep}(t) = \frac{k_{deep}\dfrac{dw}{d\phi}}{d_{EMPD-deep}}\phi_{ZONE,f} \quad \text{(A.24)}$$

We recognize this as the same form as the equation for the surface layer. Thus, the final equation for $w_{deep}(t)$ and $M_{v,deep}(t)$ are:

$$w_{DEEP}(t) = \frac{dw}{d\phi}\phi_{ZONE,f} + \left(\frac{dw}{d\phi}\phi_{ZONE,f} - \frac{dw}{d\phi}\phi_{ZONE,i}\right)\left[1 - exp\left(-\frac{k_{deep}}{d_{EMPD-deep}}t\right)\right] \quad \text{(A.25)}$$

$$M_{v,DEEP}(t) = Ad_{EMPD-deep}\frac{dw}{d\phi}\left(\phi_{ZONE,f} - \phi_{ZONE,i}\right)\left[1 - exp\left(-\frac{k_{deep}}{d_{EMPD-deep}}t\right)\right] \quad \text{(A.26)}$$

Because the tests are measuring the absorption by both the surface layer and the deep layer, we compare the *total* moisture absorption to the data during the deep-layer tests. This total moisture absorption is:

$$M_{v,TOTAL}(t) = M_{v,SURF}(t) + Ad_{EMPD-deep}\frac{dw}{d\phi}\left(\phi_{ZONE,f} - \phi_{ZONE,i}\right)\left[1 - exp\left(\frac{-k_{deep}}{d_{EMPD-deep}}t\right)\right] \quad \text{(A.27)}$$